

# Lab on a Chip

Accepted Manuscript



This is an *Accepted Manuscript*, which has been through the Royal Society of Chemistry peer review process and has been accepted for publication.

*Accepted Manuscripts* are published online shortly after acceptance, before technical editing, formatting and proof reading. Using this free service, authors can make their results available to the community, in citable form, before we publish the edited article. We will replace this *Accepted Manuscript* with the edited and formatted *Advance Article* as soon as it is available.

You can find more information about *Accepted Manuscripts* in the [Information for Authors](#).

Please note that technical editing may introduce minor changes to the text and/or graphics, which may alter content. The journal's standard [Terms & Conditions](#) and the [Ethical guidelines](#) still apply. In no event shall the Royal Society of Chemistry be held responsible for any errors or omissions in this *Accepted Manuscript* or any consequences arising from the use of any information it contains.

## **3D-printed Fluidic Networks as Vasculature for Engineered Tissue**

Ian S. Kinstlinger and Jordan S. Miller, Ph.D.\*

Department of Bioengineering, Rice University, Houston, TX, USA

\* Corresponding author (jmil@rice.edu)

## Abstract

Fabrication of vascular networks within engineered tissue remains one of the greatest challenges facing the fields of biomaterials and tissue engineering. Historically, the structural complexity of vascular networks has limited their fabrication in tissues engineered *in vitro*. Recently, however, key advances have been made in constructing fluidic networks within biomaterials, suggesting a strategy for fabricating the architecture of the vasculature. These techniques build on emerging technologies within the microfluidics community as well as on 3D printing. The freeform fabrication capabilities of 3D printing are allowing investigators to fabricate fluidic networks with complex architecture inside biomaterial matrices. In this review, we examine the most exciting 3D printing-based techniques in this area. We also discuss opportunities for using these techniques to address open questions in vascular biology and biophysics, as well as for engineering therapeutic tissue substitutes *in vitro*.

## Introduction

The networks of blood vessels that comprise the circulatory system have enthralled scientists for hundreds of years with their exceptional intricacy. The elegant branching patterns of the vasculature, optimized to meet the needs of neighboring tissues, showcase the conserved architectural features observed throughout nature where fluid transport is required. For example, we consider the complete vasculature of the heart (Fig 1). Vasculature in the heart exhibits smooth hierarchical branching in three dimensions, all the way from the centimeter-scale (aorta) to the micron-scale (capillaries). Recapitulating this complexity *in vitro* has become a

fundamental challenge in the ongoing effort to engineer living tissues. At this time, techniques capable of fabricating native vascular architecture within living tissue have not yet been demonstrated. In particular, no single technique can currently capture such complexity at the various length scales of vasculature. Until methodology advances in this area, engineered tissue equivalents for the solid organs (e.g. lung, liver, kidney) are unlikely to become reality.

Recent reviews and commentaries have noted the critical role of vascular networks in developing functional tissue equivalents and called for techniques to fabricate vascular networks in engineered tissue.<sup>1-3</sup> Oxygen transport is the limiting factor for survival of cells at high-cell densities in three-dimensional (3D) environments, yet oxygen diffusion is limited to 150-200  $\mu\text{m}$ . Thick tissues ( $>400 \mu\text{m}$ ) containing physiologic cell densities therefore develop a necrotic core in the absence of vasculature.<sup>4</sup> Tissues without fluid-carrying channels also lack a mechanism for supplying cells with nutrients and removing  $\text{CO}_2$  and cellular waste. Additionally, the vasculature is an important conduit for the influx of circulating cells and bioactive factors into tissue.<sup>1</sup> Finally, other fluidic networks contribute essentially to tissue function; for example, lymphatic vessels are needed to regulate interstitial fluid volume and lung bronchioles are needed for blood oxygenation. Until these structures can be fabricated, engineered tissues will not recapitulate the functions of their native counterparts.

Recently, numerous approaches have emerged to meet this urgent need within the field. Advances in microfluidics enabled fabrication of fluidic networks in plastic resins with architectural features reminiscent of vasculature. While these materials differ considerably from the materials that have gained the attention of biomaterials and tissue engineering researchers, the architectures are compelling nonetheless. Additionally, some investigators have used conventional microfluidics techniques in conjunction with biomaterials to create fluidic channels and networks

relevant to tissue engineering.<sup>5-9</sup> Outside of traditional microfluidics, a variety of 3D printing techniques have been developed for fabrication of fluidic networks. 3D printing (3DP, also known as additive manufacturing) refers to a suite of fabrication technologies that additively create geometries layer-by-layer in 3D space, including inkjet printing<sup>10</sup>, extrusion-based printing<sup>11</sup>, Selective Laser Sintering/Melting<sup>12,13</sup>, and stereolithography<sup>14</sup>. As we will illustrate, these techniques are enabling freeform fabrication of complex fluidic networks within biomaterial matrices.

A unifying feature of the strategies described above is the treatment of the vasculature simply as a network of fluid-carrying channels. Thus, spatial patterning of vascular architecture is decoupled from the complex biology of the vessels. Using many of the techniques described below, it is possible to study the same vascular architecture in disparate biological contexts, depending on the biomaterials and cell populations used during the fabrication process and the culture conditions used subsequently. This is useful for therapeutic tissue engineering because it enables construction of tissues with diverse cell types and bioactive factors using the same patterning techniques. Decoupling vascular architecture from biology is also advantageous in the more general case of engineered *in vitro* tissue models. Tightly controlled experiments can be designed using these models to investigate myriad biological and biophysical phenomena, as we discuss below. Here, we focus on 3DP-based techniques that have been introduced in recent years, which represent a promising set of tools to facilitate engineering of vascularized tissues *in vitro*, as well as investigation of the biology, physiology, and biomechanics of the vasculature. In this review, we highlight engineering challenges in vascular tissue engineering that may be met through 3DP and we provide a detailed literature survey of methods for 3D printing fluidic

networks. We emphasize an extensive discussion of overarching biological and biophysical questions that could be addressed using these tools.

## Length scales in the vasculature

Native vasculature follows a characteristic hierarchical branching motif, with parent vessels branching into successively smaller daughter vessels and capillaries. Blood vessels thus span several orders of magnitude in their diameters from capillaries (5-20  $\mu\text{m}$ ) to large arteries and veins (4-30 mm) (Fig 1). In our discussion, we classify vessels into three groups based on luminal diameter ( $\emptyset$ ): microvessels ( $\emptyset < 50 \mu\text{m}$ ), millimeter-sized vessels ( $\emptyset > 1 \text{ mm}$ ), and meso-scale vessels ( $50 \mu\text{m} < \emptyset < 1\text{mm}$ ). The wide range of physiologically relevant vessel sizes has historically required separate approaches aimed at creating vessels in each size range *in vitro*. However, through emerging methods such as 3DP, it may be possible to unify fabrication across length scales with a single technology.

Millimeter-sized vessels, typically in the form of synthetic vascular grafts, have been fabricated using traditional tissue engineering strategies such as polymer scaffolds<sup>15</sup>, electrospinning<sup>16,17</sup>, cell-sheet engineering<sup>18</sup> and culture in bioreactors<sup>19,20</sup>, as well as through 3DP.<sup>21,22</sup> At this length scale, vessels can be created and manipulated by hand: for example, by casting a tubular hydrogel in a mold<sup>20</sup>, by sewing a polymer mesh into a tube<sup>15,23</sup>, or by rolling up an engineered cell sheet<sup>18</sup>. In contrast, constructing microvasculature typically requires self-assembly of endothelial and supporting cell populations. Thus, efforts to engineer microvasculature have relied heavily on controlling cell populations and extracellular matrix (ECM).<sup>24-26</sup> Fabrication of meso-scale vessels presents a unique set of engineering challenges

because meso-scale vessels are too large to form via self-assembly of relevant cell types or by lithographic methods such as SU-8 photolithography, yet too small to be formed via rolled cell sheets or meshes. Furthermore, vasculature at the meso-scale consists not of isolated vessels (akin to millimeter-sized vascular grafts), but of connected, branching networks embedded within a bulk ECM.

Here, we focus on emerging techniques for fabricating fluid networks at the meso-scale. The two most prominent strategies in this area are based on soft lithography and 3DP. These approaches are ideally suited for fabricating vessels at this length scale because of their intrinsic spatial resolution. We discuss benefits and limitations of soft lithographic approaches in the following section and propose that 3DP-based fluidic networks are an especially promising strategy for fabrication of meso-scale vessels with physiologic complexity *in vitro*.

### Vascular networks: microfluidics inside living tissue

As engineers, it is useful to simplify our view of the vasculature by focusing simply on its architecture, separating the geometric properties of vascular networks from their highly complex biology. From this perspective, key fabrication advances in the area of microfluidics may be highly applicable to constructing living vasculature. For example, perfusable 3D networks have been created in epoxy matrices (Fig 2a).<sup>27,28</sup> As the field has progressed, synthetic vascular networks have captured branching<sup>29</sup> (Fig 2b) and interpenetrating<sup>30,31</sup> (Fig 2c) architectures. Taken together, these geometries encompass many key features of native vasculature; if these networks could be created in biomaterials instead, they would be excellent *in vitro* models for vascularized tissue and potentially useful therapeutically. As a key intermediate step between plastic matrices and living

tissue, branching networks were printed within a Pluronic hydrogel<sup>32</sup> (Fig 2d). Interestingly, the architectures surveyed in Figure 2 were fabricated by removal of temporary sacrificial materials. As we discuss below, similar sacrificial templating strategies have also been implemented within biomaterials, underscoring the common goals and methodology of contemporary microfluidics and tissue engineering research. In addition to this sacrificial templating strategy, techniques have been introduced within the microfluidics field enabling freeform fabrication of fluidic networks spanning from the meso-scale<sup>8,9</sup> to the micron-scale,<sup>33</sup> which continue to serve as stimulating examples to motivate fabrication of functional vasculature.

Just as fluidic networks patterned in epoxy resins exhibit relevant architectural features for engineered blood vessel networks, other ongoing work in the field of microfluidics is also paving the way for functional engineered vasculature. In the past decade, directional fluid transport through patterned channels became commonplace in the microfluidics community; biomaterials scientists now seek directional blood perfusion through patterned vessels of similar sizes. Similarly, just as chemical gradients are now readily generated via microfluidics<sup>34,35</sup>, gradients of bioactive factors within tissue are now desired for tissue engineering studies.<sup>36,37</sup> In terms of fabrication methodology, microfluidics has traditionally relied on soft lithography workflows<sup>38</sup>, but is now transitioning towards 3DP, which offers greater 3D complexity, higher fabrication throughput, and rapid device prototyping.<sup>39-42</sup> The equivalent trend in biomaterials has been a shift from lithographic methods towards the 3DP techniques discussed here. Finally, investigators in materials science have made great strides towards the fabrication of materials which self-heal via reagents delivered through fluidic channels.<sup>30,31,43,44</sup> Analogously, there is now a great need for fluidic networks within engineered tissues through which oxygen, nutrients, and bioactive factors can be delivered.

Overall, the field of microfluidics has confronted and overcome many of the same challenges (described in the preceding paragraph) that the fields of biomaterials and tissue engineering face today. Therefore, translation of successful microfluidic techniques into biomaterials is expected to be useful for fabrication of increasingly complex vascularized tissue equivalents. Furthermore, we postulate that investigators in microfluidics have the knowledge and experience necessary to tackle many of the engineering challenges discussed in this review. Communication and collaboration between materials scientists and biologists has already helped to shape design principles for tissue engineering; continuing this dialog will be vital as we take on the great challenge of building living tissue.

### Controlling fluid convection in engineered tissues

The end goal of perfusable vascular networks in engineered tissue is to provide convective transport of nutrients and oxygen to the tissue core. However, some notable efforts to introduce fluid convection forego vessel-like channels in favor of a macroporous tissue architecture. For example, macroporous hepatocyte-laden hydrogels have been created by Tsang and colleagues and by Neiman and colleagues using additive photopatterning techniques. The convective transport afforded by macroporous architecture significantly improved hepatocyte survival and function as compared to bulk unpatterned hydrogels lacking fluid convection.<sup>45,46</sup> Macroporous architectures have also become commonplace in scaffolds for bone tissue engineering, as discussed in several thorough reviews.<sup>47-49</sup> While macroporous engineered tissues effectively facilitate nutrient transport via fluid convection, this approach is problematic in the context of clinical translation of engineered tissue. The difficulty of endothelializing highly tortuous interconnected pores compromises the hemocompatibility of macroporous engineered tissues. Furthermore, because

connected porous networks have no defined inlets or outlets, such tissues cannot readily be integrated with host vascular supply. The lack of directional fluid convection also means that fluid mechanical cues which contribute to native tissue function may be absent from these constructs.

The limitations of macroporous scaffold architectures have shifted focus towards biomaterials with living cells containing precisely patterned fluidic channel networks. Uniaxial meso-scale networks can be created through needle-molding techniques as well as through soft lithography. In needle-molding techniques, pioneered by Tien's group, hydrogels are cast around one or more steel needles; careful removal of the needles yields perfusable channels (75-150  $\mu\text{m}$ ) in the hydrogel (Fig 3a).<sup>5,50</sup> The simplicity of this approach is striking, as is its compatibility with virtually all natural and synthetic polymeric biomaterials. As we discuss below, key insights into vascular biology have already been gained through simple needle-molded meso-scale vessels.<sup>51,52</sup> Additionally, the simple network architecture of uniaxial channels facilitates computational transport modeling, followed by experimental validation.<sup>53</sup> Needle-molding is limited, however, to arrays of uniaxial channels, requiring alternate approaches as the field works towards therapeutic vascular tissue replacements and physiologically relevant models of native branching vasculature.

Soft lithographic approaches offer similar versatility to needle-molding approaches with the potential for more complex channel arrangements and higher throughput. Typically, a master is used to mold troughs in a hydrogel or elastomer (e.g. collagen or PDMS), and the trough-containing slab is bonded to a second slab to create closed channels (25  $\mu\text{m}$  to hundreds of microns; Fig 3b).<sup>37,54</sup> A highly detailed protocol for this approach was provided by Morgan and colleagues.<sup>55</sup> As with needle-molding, the simple *in vitro* models fabricated via soft lithography have already proven useful as experimental platforms for studying vascular biology.<sup>56,57</sup> However, soft

lithography requires expensive equipment, harsh processing conditions, and lengthy fabrication times. Fluidic networks in soft lithography are typically etched in Cartesian coordinates following straight  $x$ - and  $y$ -vectors to yield rectilinear channel architectures with uniform channel dimensions, unlike the 3D branching structures characteristic of native vasculature. While multiple iterations of bonding hydrogel slabs can effectively yield 3D fluidic networks,<sup>58,59</sup> alignment issues between layers hamper the practicality of this approach. Finally, soft lithography results in rectangular channels, unlike the cylindrical vessels found in the body. Rectangular channels experience heterogeneous wall shear stresses, unlike cylindrical channels, imparting non-uniform fluid mechanical cues to endothelial cells.<sup>60</sup> Right-angle intersections between channels also could introduce very different flow patterns than native branched intersections, including flow stagnation, which can impact cell seeding uniformity.<sup>61</sup> Finally, it has been noted that the dynamics of vessel occlusion vary considerable between rectangular and circular vessel cross-sections.<sup>62</sup> The above concerns are mitigated, however, by the observation that endothelial cells seeded within rectangular channels remodeled the vessel resulting in an elliptical or circular cross-section.<sup>57</sup> This remodeling effect likely depends on the stiffness of the bulk ECM surrounding the patterned channels, and has not been fully characterized.

3DP-based approaches have the potential to overcome the limitations associated with needle-molding and soft lithographic techniques. 3DP enables freeform fabrication of structures in 3D space, opening the door for complex 3D fluidic networks. The resolution of most 3D printers is on the order of hundreds of microns, making this strategy suitable for fabricating meso-scale vasculature. It is worth noting that several 3DP techniques have been developed with an open-source philosophy, making these biofabrication tools highly accessible to the community and, in some cases, surprisingly inexpensive.<sup>63,64</sup> In the following section, we provide a thorough review

of 3D-printed fluidic networks encompassing the diverse approaches that have been introduced in recent years.

### 3D Printing approaches for fabricating vascular networks

3DP of fluidic networks for tissue engineering has relied primarily on extrusion-based printing and stereolithography. Extrusion-based 3DP additively creates geometry by dispensing material through an extruder while a computer-controlled 3-axis gantry moves the extruder to the appropriate position in 3D space. A fundamental challenge in direct extrusion printing of fluidic networks is the tendency of small-diameter channels to fold or collapse under their own weight, particularly in the case of overhanging channels. Thus, extrusion printing is often not truly freeform in all three dimensions. This hurdle can be overcome by printing in the presence of a support material, which is separated from the print structure once printing finishes. Fluidic networks can also be fabricated using extruded sacrificial templates. In sacrificial templating, the template structure is fabricated in a temporary material and encased in a second bulk material. Selective removal of the temporary material yields a fluidic network in the bulk material which retains the architecture of the original template. Sacrificial templating is not exclusively associated with 3D-printed templates: Golden and Tien used a PDMS mold to create a bifurcating gelatin template, around which hydrogels were cast. Liquefying, then removing the gelatin enabled the construction of fluidic hydrogels with landmark complexity.<sup>59</sup>

The literature related to extrusion-based 3DP of fluidic networks is complemented by a growing body of work which utilizes light as a patterning tool for additive fabrication. Generally referred to as stereolithography (SLA), light-based 3DP additively creates structures by solidifying

a liquid material layer-by-layer in a photochemical reaction. In conventional SLA, the light source is a laser, which raster scans across the liquid starting material to solidify it in a desired pattern. In projection SLA (also known as digital light processing, DLP) a pattern of light and dark pixels is projected onto the liquid starting material, which solidifies where exposed to light pixels. Photopatterning offers several key advantages specific to bioprinting. The resolution of SLA, determined by the laser spot size or projector pixel size, is generally higher than that of extrusion-based methods, and potential cell injury/death due to high shear stress during extrusion is avoided. Conversely, photopatterning is limited to photopolymerizable materials (e.g. poly(ethylene glycol) (PEG) acrylates), and printing protocols must be designed to minimize phototoxicity or excessive exposure to photoinitiator.<sup>65</sup>

### **3D Printing uniaxial channel arrays**

The simplest 3D-printed fluidic networks are arrays of uniaxial channels, similar to the channels produced through needle molding or soft lithography, as discussed above. The Dai group has constructed uniaxial meso-scale fluidic channels in hydrogels using gelatin sacrificial templates. Collagen and gelatin were co-extruded such that a fiber of gelatin (~1 mm) was encased in a bulk collagen matrix (Fig 3c).<sup>66,67</sup> Removal of the sacrificial gelatin template was facilitated by the phase transition from solid to liquid gelatin above 37 °C, and the resulting open fluidic channel supported flow perfusion. An interesting aspect of this work was the encapsulation of ECs within the sacrificial gelatin template, which migrated through the liquefied gelatin and adhered to the collagen channel wall. Functionally, however, it does not appear that introducing ECs in this manner leads to a different outcome than seeding them directly inside open channels. Wüst and colleagues used a similar approach – sacrificial gelatin fibers printed within a bulk alginate matrix

– to fabricate fluidic channels with architectures of greater complexity than a single channel.<sup>68</sup> Channels of variable width were formed, as were intersecting channels, channels with turns, and channels printed in a vertical orientation.

Arcaute, Mann, and Wicker used laser-based SLA to pattern an array of uniaxial channels in PEG-dimethacrylate (PEG-DMA) hydrogels in an early example of photopatterned hydrogels (Fig 3d).<sup>69</sup> When fibroblasts were added to the PEG-DMA pre-polymer solution (with covalently incorporated RGDS peptide), excellent viability was observed after 24 hours of encapsulation in the polymerized gel. In a subsequent study, the authors showed that multiple materials could be patterned side-by-side in channel-containing hydrogels.<sup>70</sup> The implications of multi-material hydrogels are far-reaching; in theory, simultaneous printing of multiple materials could allow fabrication of engineered tissues with heterogeneous internal organization of cells and ECM, which could more accurately model native tissue organization. Similar work by Suri and colleagues used projection SLA to fabricate vertical channels in a modified hyaluronic acid matrix.<sup>71</sup> The authors further demonstrated that gradients of molecules could be patterned along the length of channels during printing and hypothesized that such gradients could be useful in printed nerve guidance conduits.

Raman and colleagues recently introduced a projection microstereolithography ( $\mu$ SLA) technique using greyscale projected patterns to 3D print positive and negative features in PEG with feature resolution  $<10\ \mu\text{m}$  ( $<30\ \mu\text{m}$  after equilibrium PEG swelling), as well as open fluidic channels with  $100\ \mu\text{m}$  diameter (Fig 3e).<sup>72</sup> The authors further demonstrated printing successive layers with different materials as well as fibroblast encapsulation surrounding patterned fluidic channels. As exemplified by this work, SLA methods are capable of producing extremely high-resolution features and fluidic channels, but with architectural complexity still largely restricted to

uniaxial channels. If investigators using SLA-based fabrication can extend their techniques to complex 3D network architectures, SLA is poised to become perhaps the most versatile approach for 3D printing fluidic networks. Furthermore, recently introduced Continuous Liquid Interface Production (CLIP) marked a landmark advance in light-based additive manufacturing, offering monolithic printed parts with unprecedented efficiency.<sup>73</sup> Recently, continuous projection printing was demonstrated with PEG-Diacrylate, leading to the efficient production of concave microstructures.<sup>74</sup> However, there are still major obstacles associated with using this process to print fluidic networks in arbitrary orientations. Because typical biopolymer printing materials are optically transparent, open channels (i.e. regions not exposed to light) become exposed to light during polymerization of subsequent layers. Thus, unreacted polymer residing in the channels can become crosslinked as the printing process continues, thereby occluding the channel. If continuous projection 3DP of biocompatible materials could be extended to open fluidic channels, the rapid fabrication process would facilitate scaling up the size of engineered vascularized tissues.

### **Fluidic networks with lattice architecture**

Rectilinear lattices represent a step up in complexity from uniaxial channels arrays because they enable fluid transport along multiple axes and can include junctions between channels. Intervessel junctions are the basis for vascular architectures which terminate in a single inlet and outlet, making these lattice geometries relevant for studying flow patterns at branch points. In one paradigm for direct extrusion of lattice networks, coaxial extrusion nozzles are employed to produce free-standing fluidic channels (Fig 4a). The outer nozzle contains an uncrosslinked biopolymer (e.g. alginate or chitosan) while the inner nozzle contains the corresponding crosslinker (e.g. calcium chloride or sodium hydroxide). Local crosslinking at the interface

between polymer and crosslinker creates freestanding crosslinked channels, where extrusion rates control channel dimensions. This technique has been used by Ozbolat's group to create channels with inner diameter  $<200\ \mu\text{m}$  and outer diameter  $<500\ \mu\text{m}$ .<sup>75</sup> The freestanding alginate channels can be printed in a rectangular grid, allowing fluid transport along two axes, then encapsulated within bulk hydrogels. Importantly, the encapsulation step is material agnostic – essentially any natural or synthetic extracellular matrix (ECM) can be used. Another key insight by the authors was the ability to co-encapsulate multiple free-standing channels in the same hydrogel and use the separate channels to independently deliver two different fluids to various regions of the gel. Using this approach, cells have been encapsulated in freestanding alginate channels with excellent viability and evidence of collagen deposition.<sup>76–78</sup> Luo, Lode, and Gelinsky used a similar method to construct hollow-fiber scaffolds with alginate in a log cabin architecture such that each successive alginate fiber layer was oriented perpendicular to the previous layer.<sup>79</sup> In other studies, alginate channels were supplemented with carbon nanotubes to improve mechanical strength cite.

In a different implementation of coaxial nozzle extrusion, Colosi and colleagues printed a grid of solid alginate/methacrylated gelatin (GelMA) fibers by extruding alginate/GelMA prepolymer through the inner nozzle and calcium chloride through the outer.<sup>80</sup> Covalent photocrosslinking of the GelMA reinforced the fibers following printing. Over the course of ~5 days, however, the ionically crosslinked alginate disintegrated to leave hollow fluidic channels with interconnected filaments (Fig 4b). Furthermore, endothelial cells (EC) suspended in the prepolymer became encapsulated in the crosslinked fibers and migrated to the edges of the fibers, forming an endothelial monolayer (possibly encouraged by the disintegration of the alginate component). Thus, it is possible to pre-fabricate an endothelialized fluidic network, then subsequently cast a bulk tissue around this network.

We introduced a method for sacrificially templating meso-scale fluidic lattices using extruded carbohydrate glass.<sup>64</sup> The size of the glass filaments can be directly controlled by the lateral nozzle speed to yield filaments in the 150-750  $\mu\text{m}$  range. Lattices composed of these filaments are free-standing and can be encased in various natural and synthetic ECM materials (Fig 5c). Subsequent removal of the sugar glass is accomplished simply by dissolving in water, then flowing out the dissolved glass. Carbohydrate glass templates are sufficiently stiff to be self-supporting, such that the bulk matrix does not need to be printed alongside the template, but can be cast around it afterwards; thus, this technique is not limited by the feasibility of printing a particular ECM material. We further found that fluidic networks fabricated via carbohydrate glass templating were stable under applied pulsatile flow, were amenable to endothelialization, and improved cell viability in 3D fibrin gels compared to slab gel controls. Diverse planar lattice networks have been formed with this method including curved filaments; however, the technique is not as successful at freeform printing in all three dimensions.

### **3D branching fluidic networks**

Branching networks exhibit the highest level of complexity achieved so far for fluidic networks within biomaterials. Hierarchical branching is the architectural signature of native vasculature and central to the efficient transport of oxygen and nutrients. The ubiquity of branching networks is attributed to the fact that this architecture minimizes the resistance to flow.<sup>81,82</sup> Thus, the early examples of branching networks discussed here represent the closest efforts yet to mimic the complexity that pervades tissues in the body. For example, Christensen and colleagues 3D-printed bifurcating fluidic networks by inkjet deposition of alginate droplets into a supporting bath of calcium chloride (Fig 5a).<sup>83</sup> The calcium chloride bath serves as an ionic crosslinker for the

alginate and the buoyant force exerted on the alginate droplets (due to density differences) supports the formation of complex overhangs and spanning regions. Use of a liquid-phase support material makes separation of the support material from the printed alginate trivial.

A multi-photon variant of SLA was employed by Meyer and colleagues to pattern extremely small-diameter fluidic tubes and bifurcating channels. The especially high resolution of multi-photon stereolithography enabled the fabrication of branched tube structures with 18  $\mu\text{m}$  luminal diameter and wall thickness  $<5 \mu\text{m}$ , using a polytetrahydrofuranether-diacrylate (Fig 5b).<sup>84</sup> Also using SLA, Arcaute and colleagues printed branching channels with defined inlet/outlet within a bulk PEG-DMA gel, highlighting the potential for SLA-based methods to produce branched fluidic network architectures without the need for a sacrificial template or support material.<sup>69</sup>

Direct extrusion 3DP has been used to print complex branching networks within a supporting slurry of hydrogel microparticles. Rheologically, this slurry behaves as a Bingham plastic, fluidizing from its solid resting state when applied shear stress crosses a threshold (physically, the transition between solid and fluidized states is referred to as a jamming/unjamming transition<sup>85,86</sup>). Shear-induced fluidization of a granular slurry can be exploited for extrusion 3D printing: the extrusion nozzle is free to move through the slurry as its motion exerts fluidizing shear on the granules, but deposited material is locked into place as the slurry solidifies in the wake of the nozzle. Bhattacharjee and colleagues extruded PDMS, photoreactive poly(vinyl alcohol) (PVA), and collagen structures within a slurry of Carbopol particles<sup>85</sup>. PVA was crosslinked after printing and fully crosslinked structures were recovered from the Carbopol slurry by immersion in stirred water. Highly complex structures were printed using this system, including hierarchically

branching networks (Fig 5d). Concentrically nested objects were also printed, highlighting the potential for this technique to produce biological structures with heterogeneous internal structure.

Hinton and colleagues introduced a similar approach using a support bath of gelatin hydrogel microparticles, which the authors refer to as Freeform Reversible Embedding of Suspended Hydrogels (FRESH).<sup>63</sup> The authors demonstrated FRESH printing with alginate, fibrin, and collagen, where alginate and fibrinogen were crosslinked by infusing the gelatin slurry with calcium chloride and thrombin, respectively. The gelatin slurry can be liquefied with an increase in temperature to 37 °C, thereby liberating the embedded printed hydrogel. FRESH printing was used to produce physiologically relevant structures with highly complex architecture, including a branching arterial tree (Fig 4e) and a 3D-scanned embryonic chick heart with internal trabeculae. Overall, granular gel and FRESH printing facilitate construction of the most geometrically complex hydrogel structures yet presented in the field.

Sacrificial agarose templating was demonstrated for fabrication of meso-scale branching networks by Bertassoni and colleagues. Gelled agarose fibers were extruded in the pattern of desired fluidic networks, then encased in naturally derived (GelMA) or synthetic (various PEG) hydrogels.<sup>87</sup> The authors found that the agarose fibers could be readily removed under light vacuum to yield open, perfusable channels spanning 250-1000  $\mu\text{m}$  diameter (Fig 5f). Branching fluidic channels were formed by depositing separate fibers for each branch which converge at the branch point. The authors went on to show that ECs seeded inside the channels proliferated and formed a mature endothelium, evidenced by cell junctions. Viability and alkaline phosphatase expression of MC3T3 cells was significantly higher in gels with channels than in block gels, presumably owing to improved oxygen/nutrient transport.

Finally, a sacrificial templating method was introduced by Kolesky and colleagues, where a temporary (fugitive) template for fluidic channels is printed in Pluronic F127 alongside cell-laden ECM.<sup>88</sup> Pluronic F127 (Pluronic) is a triblock copolymer of PEG and poly(propylene oxide) (PPO) which liquefies below 4 °C and has been used previously as a fugitive ink<sup>29,32</sup>. Pluronic was printed in various architectures including rectilinear lattices, bifurcating branches, and 3D zigzags, then liquefied and removed in each case to yield a perfusable fluidic network (Fig 5e, channel diameters 100-1000 μm). In practice, Pluronic is deposited alongside the bulk ECM, which acts as a support material.

Two recent groundbreaking studies employed sacrificial Pluronic extrusion to create vascular networks within large-scale engineered tissue constructs. Kolesky and colleagues extruded Pluronic and thrombin alongside a cell-laden ink composed of gelatin, fibrinogen, fibroblasts, and mesenchymal stem cells (MSC).<sup>89</sup> Evacuation of Pluronic followed by perfusion of ECs led to endothelialization of vascular channels. The authors showed survival and osteogenic differentiation of MSCs deep within the construct over 6 weeks, enabled by convective oxygen, nutrient, and bioactive factor transport through the templated vascular networks. Separately, Kang and colleagues extruded Pluronic alongside two cell inks (also gelatin/fibrinogen-based) as well as polycaprolactone, which served as a mechanical support.<sup>90</sup> Bone, cartilage, and skeletal muscle tissues, with architectures derived from clinical imaging data, were all printed using this co-extrusion system. The authors demonstrated that fluidic channels formed by sacrificial Pluronic templating enhanced cell survival and tissue formation by overcoming transport limitations associated with diffusion. These recent reports present compelling evidence that through incorporation of 3D-printed fluidic networks, the size, structural complexity, and functional performance of engineered tissues can be expected to increase dramatically in the coming years.

## Applications and Future Outlook for 3D-printed Vascular Networks

Historically, the fabrication of fluidic networks in biomaterial matrices has been a major challenge, but exciting new solutions have been developed in the past several years, raising the critical question of how to effectively use these techniques to interrogate biological and biophysical phenomena as well as build functional engineered tissues. Below, we review studies that have been conducted with the aid of engineered fluidic networks in four areas: vascular physiology, tissue function and organization, disease models, and tissue engineered therapeutics. The types of discoveries outlined here illustrate the power of *in vitro* models containing fluidic networks and suggest how the field will continue to benefit from these models. It is important to note that there is no clear consensus on what minimum requirements constitute functional vasculature. Indeed, there are many possible answers. For example, by some definitions, channels with patent lumens might satisfy the definition of functional vasculature. Yet, by other definitions, vasculature might require organized ECs, supporting cells, and smooth muscle cells to be recognized as functional. Through the future directions described below, a clearer definition of what exactly constitutes functional vasculature may become evident.

### Vascular Physiology and Fluid Mechanics

By employing endothelialized fluidic channels as models for blood vessels, many investigators have gleaned previously appreciated knowledge about angiogenesis, vessel stability, and vessel function. For example, Zheng and colleagues used endothelialized channels with pericytes seeded in the bulk ECM to elucidate a relationship between pericyte density and endothelial sprouting<sup>57</sup>. Other studies used similar techniques to show that cell density and vascular geometry influence sprouting<sup>36</sup> and that a threshold exists beyond which shear stress

induces angiogenesis<sup>51</sup>, mediated by ECM stiffness<sup>91</sup>. Based on these early studies, patterned fluidic networks are likely to be useful for answering the many remaining questions surrounding the complex process of angiogenesis. For example, these models could help validate systems biology models for signaling in angiogenesis<sup>92,93</sup>, interrogate the role of angiogenesis in cancer progression, or design treatment plans for pro- or anti-angiogenic therapies.

Vascular stability and barrier function have also been studied with *in vitro* endothelialized channel models, including several prominent studies by Tien's group. For example, endothelial delamination and vessel leakage, typical during culture with standard growth media, were mitigated by culture with dextran or hydroxyethyl starch.<sup>94</sup> In the same model, cyclic AMP was shown to enhance the barrier function of blood<sup>52</sup> and lymphatic<sup>95</sup> vessels, accompanied by an increase in VE-Cadherin expression. Importantly, these studies are consistent with other work *in vitro* and *in vivo*<sup>96</sup> and could be important for stabilizing engineered vasculature. Future studies in this area could examine the effects of fluid dynamics on vascular stability *in vitro* or other signaling events involving endothelial, pericyte, or smooth muscle cells. On a related note, the issue of EC thrombogenicity has been studied *in vitro* only to a limited extent, with confounding findings.<sup>97</sup> Work by McGuigan and Sefton showed that collagen hydrogels covered with an EC monolayer delayed clotting when compared to exposed collagen<sup>98</sup>. The authors reached this finding using gels exposed to blood flow. Therefore, it has been proposed that 3D-printed, endothelialized fluidic networks represent an experimental platform for more detailed investigation of thrombogenicity *in vitro*.<sup>60</sup> Unanswered questions about the influence of vascular architecture, EC sources, ECM materials, and blood fluid mechanics on thrombosis could be resolved through these techniques. Because shear stress plays a critical role in platelet adhesion<sup>99,100</sup>, cylindrical 3D-printed fluidic

channels and their associated homogeneous, physiologic shear stress patterns are ideal for further study in this area.

Engineered vascular networks also provide a rich opportunity to investigate the fluid dynamics of blood flow within tissue. In nature, it is difficult to probe the influence of vascular network architecture on fluid dynamics because only observational studies are possible using naturally occurring architectures. 3D printing, however, could be used to fabricate vascular networks with different geometric parameters (e.g. branching angle, branching frequency, tortuosity), enabling controlled experiments of fluidic dynamics as a function of architecture. Computational fluid dynamics, particle image velocimetry<sup>91</sup>, laser Doppler imaging,<sup>101</sup> and/or laser speckle contrast imaging<sup>102</sup> could be used in concert to predict and map the flow velocities associated with a particular set of parameters. These same techniques could be used to correlate velocities and shear stresses with viability, differentiation, or migratory responses in vascular or parenchymal cell populations, providing a platform to test hypotheses in the area of vascular fluid dynamics. Because many of the 3DP techniques described here are compatible with various ECM materials, these methods also are expected to permit studies examining how ECM composition, stiffness, anisotropy, or hydraulic permeability impact vascular fluid dynamics and tissue response. To our knowledge, fluid flow has not been mapped in complex physiologically relevant branching networks at this time. It is likely that many of the investigators best suited to study fluid dynamics in engineered vasculature lack the resources or expertise to fabricate the necessary fluidic networks, and vice versa. Therefore, collaboration between fabrication experts and fluid dynamics researchers may combine the perspectives necessary to make impactful progress in this area.

Vessel anastomosis refers to the process by which two blood vessels interact and become fluidically connected. The phenomenon of anastomosis has been studied substantially *in vivo*<sup>24,103,104</sup>, but much less comprehensively *in vitro*, leaving unresolved the dynamics of how engineered vessels might fluidically connect to one another. For example, it was shown that a wrapping-and-tapping mechanism is responsible for anastomosis *in vivo*.<sup>103</sup> However, it is not certain whether this same mechanism is at play *in vitro*. Importantly, imaging experiments are not sufficient to prove the occurrence of anastomosis; fluidic connectivity must be demonstrated, typically by perfusion of fluorescent beads or dyes. Recent work by Diaz-Santana and colleagues underscores the complexity of interactions between developing vessels *in vitro* and gives early evidence for anastomosis between microvessels arising separately from vasculogenesis and angiogenesis.<sup>105</sup> Fluidic networks in hydrogels offer an excellent model system to continue probing the circumstances under which anastomosis occurs *in vitro*, as well as the mechanisms and dynamics underlying the process.

As a final example of vascular physiology which could be better understood through patterned fluidic networks, we consider the role of pericytes in stabilizing neovessels and mediating endothelial remodeling. It has been shown, mostly through *in vivo* studies, that vessel maturation and stability is pericyte-dependent and that pericytes also modulate endothelial permeability and control remodeling.<sup>106–108</sup> Additional experiments *in vitro* have corroborated the critical role of pericytes in stabilizing neovessels; studies have shown that ECs alone cannot sustain long-lasting lumenized structures without pericyte support.<sup>24,25</sup> One of the primary signaling pathways responsible for pericyte-EC interaction is the angiopoietin-1/Tie2 pathway, which promotes endothelial remodeling, inhibits apoptosis, and improves barrier function.<sup>109</sup> Angiopoietin-1 is produced by pericytes and binds to the Tie2 receptor expressed by nearby

endothelial cells. This signaling promotes EC remodeling, inhibits EC apoptosis, and decreases EC layer permeability.<sup>106,109</sup> Significant complexity arises, however, because of competing signaling from angiopoietin-2 produced by ECs. The noisy signaling environment found *in vivo* has made it challenging to isolate the dynamics and effects of this signaling, while the use of rodent models has made it difficult to generalize these findings to human vasculature. Tightly controlled experiments in 3D-printed fluidic networks containing human ECs and pericytes could validate existing findings and decouple EC-pericyte signaling from surrounding signaling events. In addition to providing fundamental knowledge of EC-pericyte interactions, these models could help us develop strategies for controlling EC behavior in engineered tissues or improve understanding of diseases involving pericyte loss, as we discuss below.

### **Tissue organization and function**

In addition to their utility for interrogating vascular physiology and biophysics, fluidic hydrogels are also promising models for understanding the organization and function of the surrounding tissue. For example, the influence of soluble factors or transport on tissue function can be studied through tightly controlled experiments in these models. Lithographically patterned channels have been used to study the influence of spatial VEGF gradients on angiogenesis<sup>36</sup> and the influence of oxygen gradients on tumor angiogenesis<sup>56</sup>. Understanding the influence of oxygen transport on tissue is especially important for tumor engineering; fluidic hydrogels may help elucidate the role of hypoxia on tumor progression. Increasingly, paracrine signaling from ECs (i.e. angiocrine signaling) is seen as a driving force for morphogenesis, cell differentiation, and tissue repair in surrounding tissues.<sup>110,111</sup> Examples include regulation of pancreatic organogenesis through signals secreted by ECs<sup>112</sup> and EC induction of liver regeneration<sup>113</sup>. Controlled fluidic

models in which ECs can interact with parenchymal cells (i.e. by paracrine signaling) could shed light on these processes and also uncover strategies for controlling the behavior of cells in engineered tissue.

Patterned fluidic hydrogels are also a promising experimental platform for studying the effects of fluid transport on tissue organization and function. In native tissue, fluid enters tissue via transmural flow out of blood vessels and exits by draining into lymphatic vessels. The resulting interstitial flow drives diverse tissue behaviors *in vivo*, including blood and lymphatic capillary morphogenesis, fibroblast differentiation, and maintenance of bone and cartilage function.<sup>114,115</sup> Interesting morphological consequences of interstitial flow have also been observed *in vitro*, including organization<sup>116</sup> and differentiation of fibroblasts<sup>117</sup> and endothelial cell morphogenesis.<sup>118</sup> The extent to which fluid convection can contribute to stability and function of engineered tissue is currently poorly understood, but may be more fully appreciated through the techniques discussed earlier in this review.

### **Disease models**

3D-printed channels have the potential to serve as models for tissue dysfunction and disease as well as healthy native tissue. Through *in vitro* disease models, investigators may gain mechanistic knowledge of disease states and develop diagnostic or therapeutic strategies.<sup>119</sup> Cancer, thrombosis/atherosclerosis, and diseases involving pericyte loss are clear candidates for modeling with the techniques discussed in this review. Tissue engineering tools for understanding cancer are growing with the advent of tumor engineering<sup>120</sup>, and combining engineered tumors with engineered vasculature offers a particularly intriguing model through which to understand the most deadly steps in cancer progression: invasion and metastasis. Kamm's group has been

especially prolific in developing *in vitro* models of tumor intravasation and extravasation by positioning cancer cells in proximity to engineered fluidic channels. Through these experiments, they have measured changes in endothelial monolayer permeability due to breast cancer cells<sup>121</sup>, characterized the time scales for tumor-EC interactions as well as the interactions themselves<sup>122</sup>, and made progress towards uncovering the still poorly understood cellular mechanisms for tumor migration.<sup>123,124</sup> These studies represent a valuable paradigm for studying cancer interactions with the vasculature.

The scalability of fluidic channel fabrication, in combination with high-throughput generation of multicellular aggregates of cancer cells<sup>125</sup>, is expected to allow us to better understand events (i.e. extravasation and intravasation) that occur infrequently *in vivo*. Additionally, it is already appreciated that fluid forces due to blood flow impact tumor intravasation and extravasation, but many of the mechanistic details are not fully understood.<sup>126</sup> Using engineered fluidic channels with controlled perfusion, experiments could be designed to elucidate relationships between hemodynamics, endothelial permeability, and extravasation/intravasation. While no two tumors have identical vascular networks, there are conserved architectural features of tumor vasculature: high tortuosity, leakiness, poor drainage function, and lack of hierarchical branching.<sup>127</sup> These dysfunctional aspects of tumor vasculature may be responsible, in part, for the poor efficacy of chemotherapy drugs.<sup>128</sup> There may be an opportunity here for 3D printed fluidic networks to enhance chemotherapy outcomes. If tumor-like vasculature could be fabricated *in vitro*, experiments could be conducted to identify ways to mitigate the deficiencies in mass transport of chemotherapy drugs. Just as *in vitro* fluidic models are expected to aid in delivering oxygen/nutrients to healthy tissues, they could also lead to strategies to improve chemotherapeutic delivery to tumors. Overall, these models are likely to be

valuable for studying mass transport phenomena within living tissue and its disruption in disease states.

Other diseases of the vasculature are also excellent candidates for further study *in vitro* in engineered fluidic networks. We have already mentioned the use of these systems to study thrombogenicity of ECs and thrombosis. Thrombosis is implicated in numerous pathological conditions of the microvasculature, so these experiments could explain fundamental mechanisms of disease as well as screen for drugs which modulate platelet adhesion.<sup>60</sup> Above, we also discussed the potential use of 3D-printed fluidic networks to study signaling between ECs and pericytes. Accordingly, pathologies involving irregular EC-pericyte signaling or pericyte loss, such as Alzheimer's<sup>129</sup> or diabetic retinopathy<sup>130</sup>, could also be better understood with these techniques. The majority of the techniques surveyed in this review (e.g. sacrificial templating techniques or hydrogel-embedded free-standing fluidic channels) offer total control over cell types, soluble factors, ECM, and fluid dynamics. Therefore, precisely engineered models of the vasculature fabricated through these techniques represent a unique platform for testing hypotheses related to pathologic signaling and aberrant pericyte loss, as well as for screening therapeutic drugs aimed at treating these conditions.

### **Therapeutic tissue engineering**

Likely the greatest motivation for fabricating physiologically relevant fluidic networks is the need to vascularize engineered tissues and organs. Successes in tissue engineering have been limited to thin tissues such as cornea, skin, and bladder; the need for vasculature to sustain tissues thicker than the 200  $\mu\text{m}$  oxygen diffusion limit has precluded progress towards engineering the solid organs (e.g. lung, liver, kidney, pancreas).<sup>4,131</sup> We are only beginning to understand how to

build fluidic networks that are structurally and functionally equivalent to native vasculature. Significant challenges that now confront the field include establishing multiscale vasculature, fabricating interpenetrating fluidic networks, connecting engineered tissues to a host vascular supply, and optimizing the design of engineered vascular networks to improve oxygen and nutrient transport *in vitro*. These advances will support the survival of physiologic cell densities,<sup>4</sup> leading up to functioning tissue substitutes.

Multiscale hierarchy is a structural motif of native vascular networks, but has only been engineered *in vitro* to a limited extent. In some studies, angiogenic sprouts have been observed to extend through the ECM between two meso-scale channels, thereby creating fluidic connection between meso-scale channels and micro-scale neovessels. For example, Nguyen and colleagues showed that under the influence of a VEGF gradient, angiogenic sprouts can bridge between two pre-formed endothelialized channels (Fig 6a).<sup>132</sup> In addition to exogenously supplied VEGF, EC-stromal cell signaling has been shown to mediate angiogenic sprouting, leading to produced multiscale vascular networks composed of a pre-formed channel and the newly formed sprouts.<sup>133</sup>

Anastomosis between 3D-printed channels and neighboring capillary beds has also been proposed to bridge meso-scale channels with microvasculature.<sup>105,134,135</sup> This strategy builds on recent separate observations of angiogenic sprouting from endothelialized fluidic networks<sup>57,64</sup> and formation of fluidically connected capillary beds via vasculogenesis.<sup>136,137</sup> Lee and colleagues provided early evidence that these two distinct cell populations can interact and that fluidic connections can form between angiogenic sprouts off of 3D-printed channels and a capillary plexus (Fig 6b).<sup>134</sup> The authors also noted intriguing trade-offs between cell viability and rates of angiogenesis and anastomosis. Similarly, Wang and colleagues showed that anastomosis occurred in a microfluidic device due to invasion of angiogenic ECs into bulk ECM containing capillaries,

in synergy with migration of lumenized ECs in the bulk gel towards the channels (Fig 6c)<sup>135</sup>. These anastomoses enabled fluidic connection between two meso-scale vessels via a capillary bed with minimal leakage (Fig 6d).

Diaz-Santana and colleagues analyzed the contributions of angiogenesis and vasculogenesis to anastomosed vessels *in vitro* and found significant intermixing of cell populations in the neovessels<sup>105</sup>. These exciting preliminary studies invite more detailed investigation of this proposed strategy for forming multiscale vascular networks. For example, the formation of multiscale networks in the presence of parenchymal cell populations has not yet been investigated, and it is unclear whether anastomosis can occur on a rapid enough timescale to sustain high cell densities in the hours and days after seeding. Furthermore, the importance of pericyte-EC signaling and fluid flow are not yet understood in the context of multiscale networks arising through a combination of angiogenesis and vasculogenesis. For example, flow has been shown to drive microvascular remodeling in the embryo<sup>138</sup>, but its role in vascular morphogenesis is currently unknown *in vitro*.

Tissues in the body contain, generally, multiple fluidic networks in an interpenetrating configuration: they weave through each other and occupy the same region of space, but are fluidically distinct (Fig 7). Arterial, venous, and lymphatic vessels are arranged in interpenetrating networks in most tissues, such that oxygen, nutrients, and interstitial fluid enter tissue through the arterial network and waste, carbon dioxide, and fluid exit through the venous and lymphatic networks. In the lungs, bronchioles and alveoli are interpenetrated by pulmonary arteries and veins; in the kidney, elaborate arterial and venous networks interpenetrate the network of collecting ducts. Interpenetrating fluidic networks are not only a hallmark of native tissue, but functionally indispensable for maintaining equilibrium of interstitial fluid volume and interstitial concentration

of nutrient and waste molecules. For example, functional loss of the lymphatic network in lymphedema causes a dramatic imbalance in interstitial fluid volume and solute transport, marked by painful swelling and accumulation of cellular debris.<sup>139</sup> *In vitro*, Wong and colleagues showed that vascular stability is compromised when interstitial fluid accumulates in the absence of lymphatic drainage due to changes in transmural pressure.<sup>140</sup> We propose that fabrication of interpenetrating fluidic networks will play a major role in advancing the field towards functional engineered tissues. At this time, no truly interpenetrating networks have been formed *in vitro*, to our knowledge. Therefore, fabrication of interpenetrating fluidic networks remains an open challenge in the field, which we believe could be addressed through the freeform fabrication capabilities of 3DP.

The increasing sophistication and technical capabilities of 3DP raises an important question: what should we be printing? It is not yet clear what fluidic networks should be printed within engineered tissue and how much complexity is needed. One possibility is direct mimicry of native vessel architecture. Using high-resolution imaging techniques such as microcomputed tomography ( $\mu$ CT), the architecture of organ vasculature can be scanned and reconstructed with the aid of appropriate software. From there, the geometry can be modified (if necessary), and 3D-printed; we recently demonstrated this workflow by 3D printing (in nylon) the architecture of mouse liver vasculature derived from a  $\mu$ CT angiography (Fig 8a).<sup>141</sup> FRESH printing was also used to print fluidic networks derived from a coronary artery MRI scan.<sup>63</sup> While it is the most direct way to recapitulate native vascular architecture, this approach could produce vascular network geometries that are difficult to print and more complex than necessary. An alternate option is printing parametric architectures designed in CAD software or through space-filling or fractal algorithms. Computational fluid dynamics (CFD) could be used to inform the design of these

geometries, enabling researchers to predict the blood flow patterns and oxygen/nutrient concentration distributions produced by a particular architecture.<sup>4,142</sup> In a simple example, CFD was used to predict the transmural pressure across an endothelialized fluidic channel depending on the placement of a drainage channel.<sup>140</sup> By integrating CFD with 3DP, closed-loop design of vascular networks becomes feasible (Fig 8b).<sup>143</sup> A candidate design can be generated efficiently through CFD predictions, then 3D-printed as a fluidic network embedded within an engineered tissue. The network design could then be refined by comparing experimental measurements of cell viability and flow dynamics with computational predictions. Iterative *in silico* and *in vitro* experiments could thus be used to optimize network architecture, facilitated by the versatility of 3DP.<sup>4</sup>

Selection of appropriate vascular architectures for engineered tissues will also require careful consideration of the fluid dynamics resulting from those architectures. As we noted above, empirical studies of fluid dynamics have not yet been conducted within complex fluidic networks 3D printed in biomaterials. However, by considering the fundamental physics of fluid flow in microfluidics (reviewed by Beebe *et al.*)<sup>144</sup> together with computational studies and experimental work in native vasculature, some simple design principles can be distilled. Likely the most widely recognized of these is Murray's Law, which was derived theoretically by determining the configuration of parent and daughter vessels which minimizes the work required to achieve flow.<sup>81,82</sup> Murray's Law states that the cubed radius of a parent vessel should equal the sum of cubed radii of its daughter branches; that is, for a parent vessel that branches into  $n$  daughter vessels,  $r_{parent}^3 = \sum_0^n r_{daughter}^3$ . This law has been widely validated in mammalian<sup>82</sup> as well as plant<sup>145</sup> fluidic networks, although more recent studies considering non-laminar flow and non-Newtonian fluid dynamics have concluded that the Murray's Law exponent is actually below 3.0.<sup>145-148</sup>

Clinically, it has been demonstrated that abnormal vessel bifurcation angles are associated with increased occurrence of peripheral vascular disease,<sup>149</sup> ischemia,<sup>150</sup> and atherosclerosis.<sup>151</sup> Specifically, bifurcations with atypical branching angles not consistent with Murray's Law experience regions of low wall shear stress,<sup>151</sup> which become sites for development of atherosclerotic plaques.<sup>152,153</sup> Thus, in the interest of mimicking the stable hemodynamics of native tissue, it seems prudent to design vascular networks in accordance with Murray's Law. We note, however, that empirical evidence does not exist for impaired cell viability or function in engineered tissues as a result of atypical branching angles. These concerns about bifurcation angle do, however, reinforce the limitations of soft lithography approaches (which generally have 90 degree branching angles) in recapitulating physiologic vessel architecture.

In addition to blood vessel branching angles and radii, other architectural parameters such as branching frequency, vessel cross-section circularity, and tortuosity are likely to be important design considerations for 3D printed fluidic networks. For example, perfectly circular 3D printed channels will have homogenous wall shear stresses, while the heterogeneous shear stresses associated with ellipsoidal or rectangular vessels might lead to non-uniformities in angiogenic sprouting, which is regulated by shear stress.<sup>154</sup> The effects of vessel tortuosity have not been well explored. Computational studies have suggested that tortuosity increases oxygen delivery;<sup>155</sup> however, it is also possible that blood or media in highly tortuous vessels will be depleted of oxygen before coming in contact with cells along the entire path length of the vasculature. Tortuous microvasculature is a hallmark of tumor mass transport;<sup>156</sup> however, the complex tumor microenvironment (e.g. high metabolic rate and hypoxia) make decoupling the impact of this tortuosity difficult. We emphasize here that while knowledge of fluid dynamics will improve

design considerations for 3D printed vascular channels, these models will also offer excellent experimental platforms to make fundamental insights about fluid dynamics.

Steady progress towards fabricating vascular networks in engineered tissues makes the vision for implantable therapeutic tissue equivalents increasingly feasible. Animal models for implantation of vascularized engineered tissue will be critical for developing implantation strategies and evaluating the function of engineered tissues *in vivo*. Unlike cell-free therapeutics or thin tissue engineered constructs, thick tissues containing vascular networks need to be directly connected to the host vascular supply. We connected PDMS gels containing fluidic networks in a rat femoral artery graft model to demonstrate a technique for rapid connection of fluidic biomaterials directly to host vasculature.<sup>101</sup> Others have explored adhesive materials to ensure robust fluidic connections between fluidic networks in hydrogels and external tubing.<sup>157</sup> Such studies are expected to inform emerging strategies for growing engineered tissues in a bioreactor or implanting *in vivo*.

## Conclusions

In the past several years, a striking array of 3DP technologies has been developed to meet the urgent need for vascular networks *in vitro*. In particular, it is now possible to print 3D heterogeneous, branched networks as both free-standing fluidic networks as well as perfusable channels within hydrogels. Through tightly controlled experiments *in vitro*, these models have already contributed significantly to our understanding of vascular biology, disease, and tissue engineering. We have outlined numerous open problems in biology, biomechanics, and bioengineering which we believe could be addressed through 3D-printed fluidic tissue models. As

the field moves forward, communication between materials scientists, biologists, and clinicians will be imperative for the design of materials and architectures which are physiologically relevant as well as amenable to *in vivo* implantation. While major challenges still lie between the current state of the field and the ultimate vision for implantable tissue substitutes, the prospect of engineering physiologic vascular architectures is beginning to appear less formidable.

## Figures

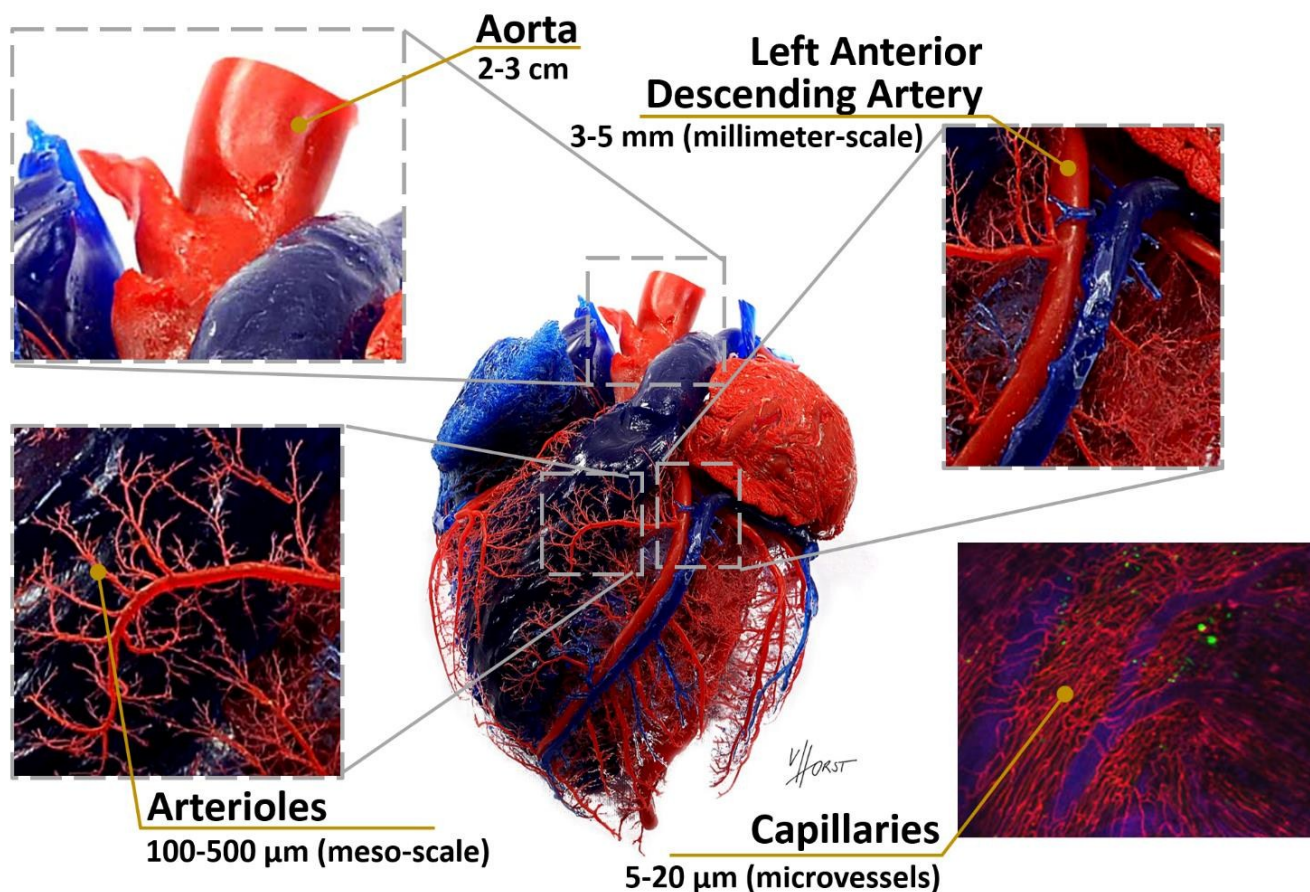


**Fig 1. The great challenge of recapitulating physiologic vasculature.** Native blood vessels span several orders of magnitude in diameter and are organized hierarchically in complex branching configurations. These elaborate networks are striking to behold, but challenging to construct *in vitro*. Because perfusable vascular networks provide vital nutrient and oxygen transport to tissue, success in building complex, large-scale engineered tissues will ultimately hinge on techniques to construct fluidic networks in biomaterial matrices, such as 3D printing. Porcine heart corrosion cast was prepared and photographed by Dr. Christoph von Horst ([www.plastinate.com](http://www.plastinate.com)) and reprinted with permission. Capillary photograph<sup>158</sup> (mouse heart; red = Rho-lectin, blue = Angiosense-680) is reprinted with permission from Nature Publishing Company.

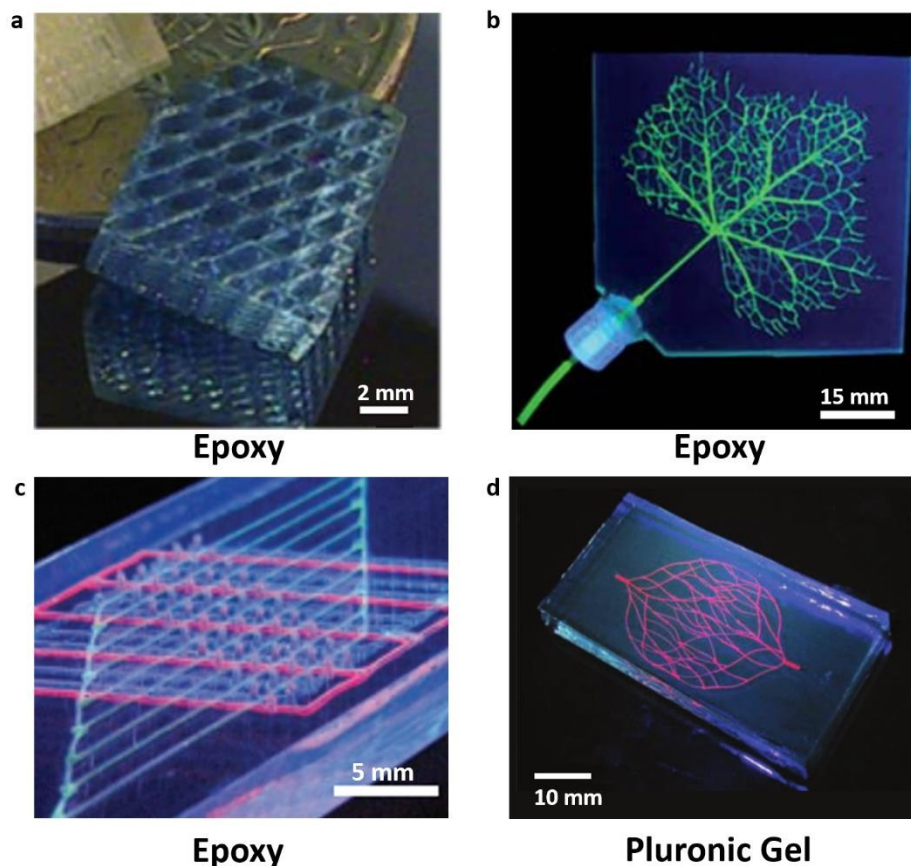


**Fig 2. Complex fluidic networks fabricated within bulk polymer matrices.** a) A 3D network of triangular-spiral towers fabricated in epoxy highlights the unique freeform fabrication associated with 3D printing.<sup>27</sup> Similar tortuous 3D networks have been used previously to promote chaotic fluid mixing.<sup>28</sup> b) This network was fabricated to mimic the leaf venation pattern of an English ivy plant, consisting of 500, 250, and 100  $\mu\text{m}$  channels in an epoxy matrix. The architecture follows Murray's Law for the angles and diameters of branching channels, in good approximation of mammalian vasculature.<sup>29</sup> c) Interpenetrating fluidic networks like this one have been investigated for construction of self-healing polymers. Here, three fluidically separate networks were patterned concomitantly to deliver epoxy resin, hardener, and thermal stabilizer to repair defects in the epoxy matrix.<sup>31</sup> d) This heterogeneous fluidic network was 3D-printed in a bulk matrix of acrylated Pluronic F127. Branching fluidic networks within Pluronic gel represent an important step in the transition from fluidic networks within polymers towards fluidic networks within living tissue. Additionally, the single inlet and outlet are important features of vascular networks designed for implantation and connection to host vasculature.<sup>32</sup> In each of these examples, the fluidic network was created by depositing a temporary sacrificial material, which was subsequently removed to obtain open channels. Reprinted with permission from John Wiley and Sons (a,c,d) and the Royal Society of Chemistry (b).

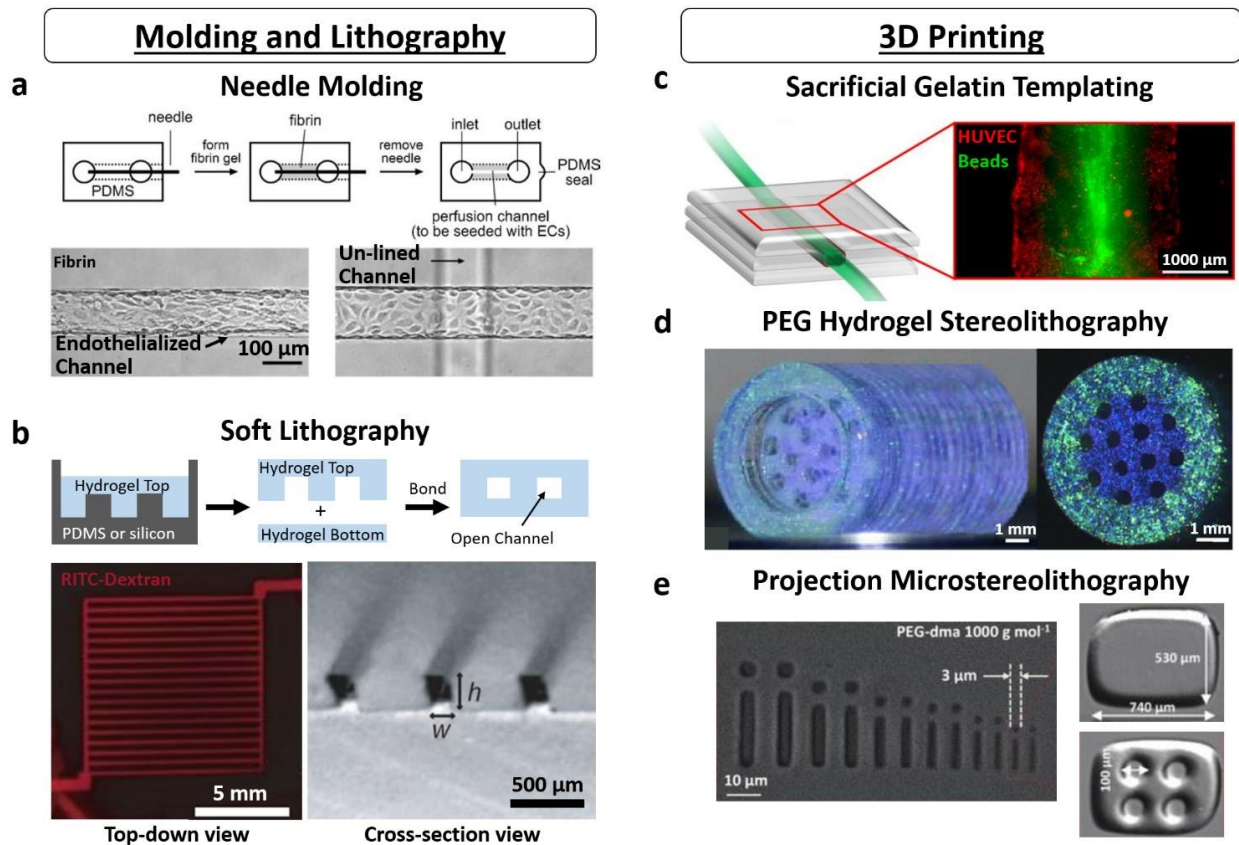


**Fig 3. Uniaxial channel arrays fabricated by needle molding, soft lithography, and 3DP.** a) A simple needle-molding technique (top schematic) creates fluidic channels in hydrogels, which can be subsequently endothelialized (bottom left). Molding channels with needles in different planes gives disconnected channels, such as the illustrated orthogonal un-lined drainage channel (bottom right).<sup>140</sup> c) In soft lithography, fluidic hydrogels are fabricated by molding with a PDMS stamp followed by a bonding process (top schematic). This workflow is compatible with complex rectilinear networks, yielding patent, perfusable vessels (bottom left). The rectangular channel cross-sections (bottom right) and right-angle channels junctions are potential drawbacks of soft lithography.<sup>54</sup> c) Gelatin extruded alongside a bulk ECM (collagen) is subsequently removed and the resulting open channel is perfused and endothelialized. The endothelial layer is stable under flow and showed mature cell-cell interactions.<sup>66,67</sup> d) PEG hydrogels containing vertical perfusable channels were fabricated by stereolithography (SLA) (encapsulated fluorescent beads for visualization). These particular structures were designed as nerve guidance conduits, but the technique is highly relevant in the context of engineered vasculature.<sup>69</sup> e) Projection  $\mu$ SLA patterns hydrogels with  $<5 \mu\text{m}$  feature resolution (left). Patterned channels with diameter  $<100 \mu\text{m}$  are also fabricated (right bottom); their increased surface area offers improved diffusion kinetics out of the gel compared to a slab control (right top).<sup>72</sup> Adapted with permission from John Wiley and Sons (a,e), the American Chemical Society (©2005, b), Elsevier Publishing Company (c), and Springer International Publishing Company (d).

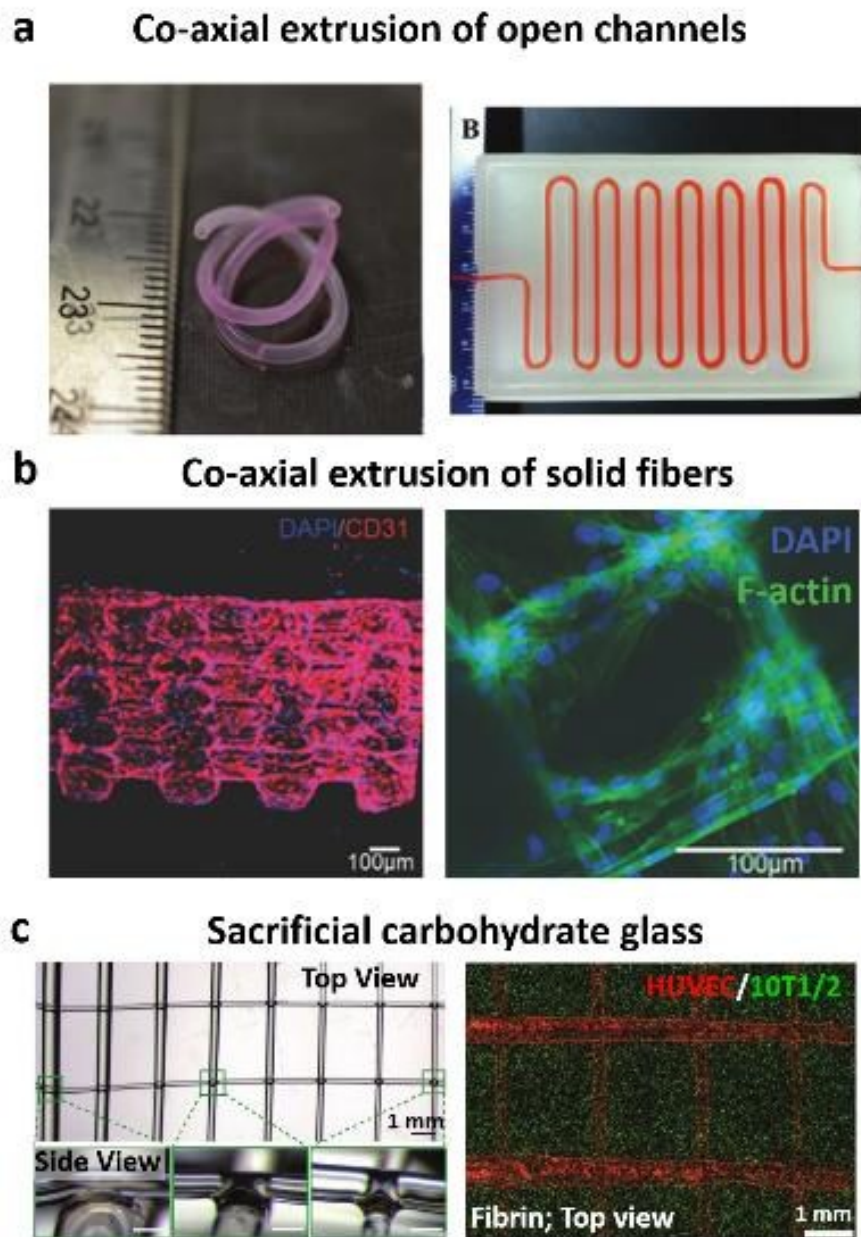


**Fig 4. 3D-printed perfusable lattices.** a) Co-axially extruded alginate forms a contiguous, free-standing fluidic channel (left) which can be printed in a rectilinear network prior to embedding in a bulk ECM (right).<sup>75</sup> b) Extrusion of alginate/GelMA fibers, followed by degradation of the alginate, yields a connected grid of open channels (left) covered with a mature endothelium (right).<sup>80</sup> c) Carbohydrate glass is extruded into lattice architectures with smooth interfilament junctions and variable filament sizes (left, side view scale bars = 200  $\mu\text{m}$ ). Encasing the glass in ECM then dissolving it away yields perfusable channels. Through this technique, independent cell populations can be seeded in the bulk ECM and lining the channels (right).<sup>64</sup> Adapted with permission from the American Society of Mechanical Engineers (a), John Wiley and Sons (b), and Nature Publishing Company (c).

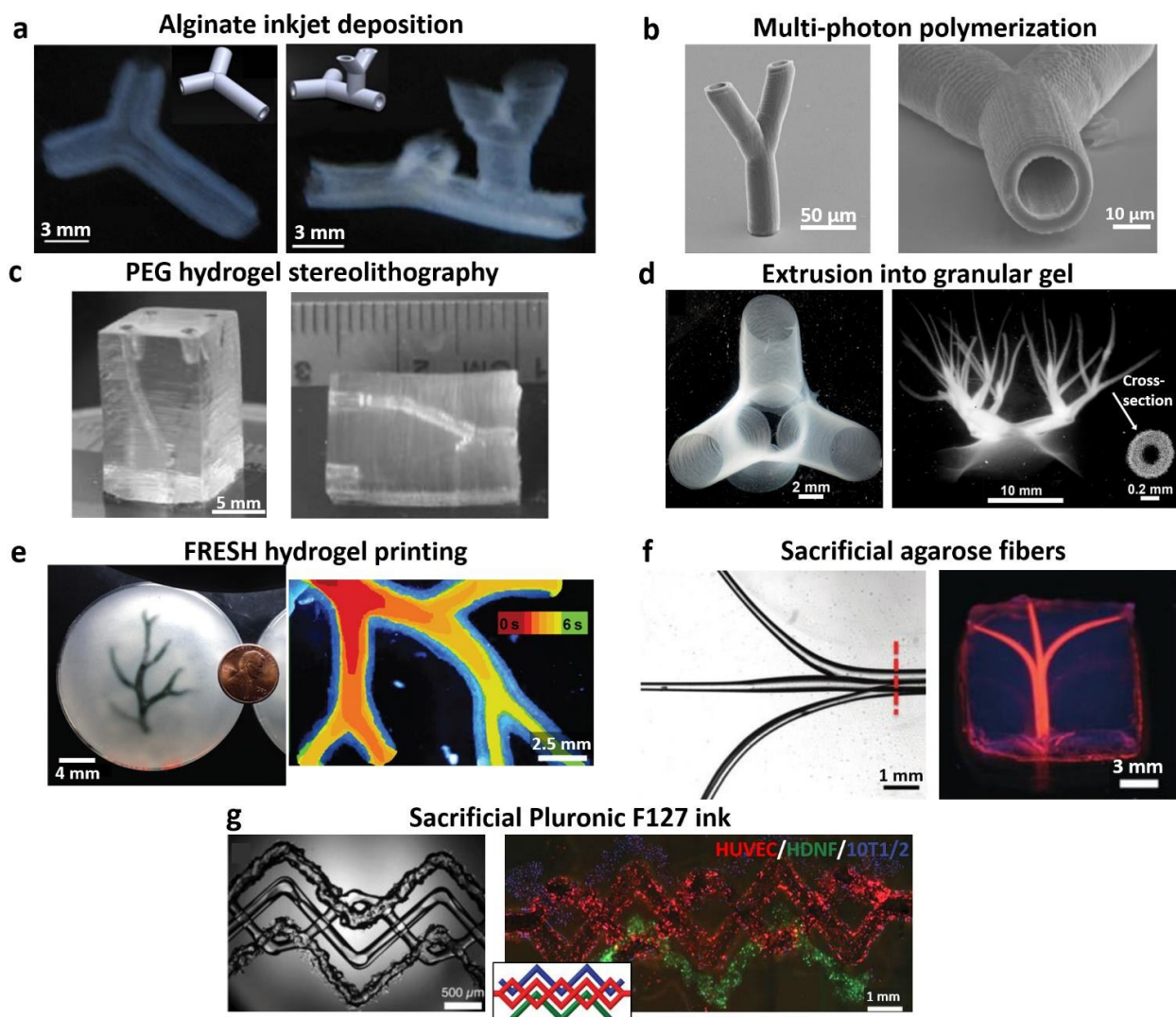


**Fig 5. Branched and complex 3D channel architectures.** a) Inkjet deposition of alginate into a calcium chloride bath allowed horizontal (left) and horizontal/vertical (right) branching free-standing fluidic channels to be printed (inset, model geometry).<sup>83</sup> b) The same stereolithographic technique used to produce uniaxial channels (Fig 3d) can also be used to create branched channels with channels in non-vertical orientations.<sup>69</sup> c) A multiphoton variant of SLA was used to create exceptionally high-resolution bifurcating fluidic channels.<sup>84</sup> d) Extrusion into a granular gel slurry allows complex fluidic networks to be fabricated, such as these hierarchically branching networks. Printed structures can be easily removed from the granular gel, as demonstrated by the right-hand model freely floating in water.<sup>85</sup> e) FRESH printing was used to deposit alginate into a gelatin slurry (left) to form the architecture of the human right coronary arterial tree. Dye perfusion through the network showed flow through all regions and bifurcations of the gel with no leaks (right).<sup>63</sup> f) 3D-printed agarose fibers printed in a branching architecture (left) were extracted from within a GelMA hydrogel to obtain the corresponding branched fluidic network.<sup>87</sup> g) Pluronic F127 ink extruded in a 3D branched zigzag (left) was evacuated from inside GelMA hydrogels, leaving the corresponding perfusable 3D channel

network. A heterogeneous cell-laden construct was obtained by printing patterns of Pluronic ink, cell-laden inks, and supporting GelMA, resulting in a 3D zigzag pattern of open endothelialized channels (HUVEC), 10T1/2 fibroblasts, and human neonatal dermal fibroblasts (HDNF) (right). Inset for the right-hand image shows the intended pattern of HUVEC, 10T1/2, and HDNF cells.<sup>88</sup> Adapted with permission from John Wiley and Sons (a,g), Springer International Publishing Company (c), and the Royal Society of Chemistry (f).

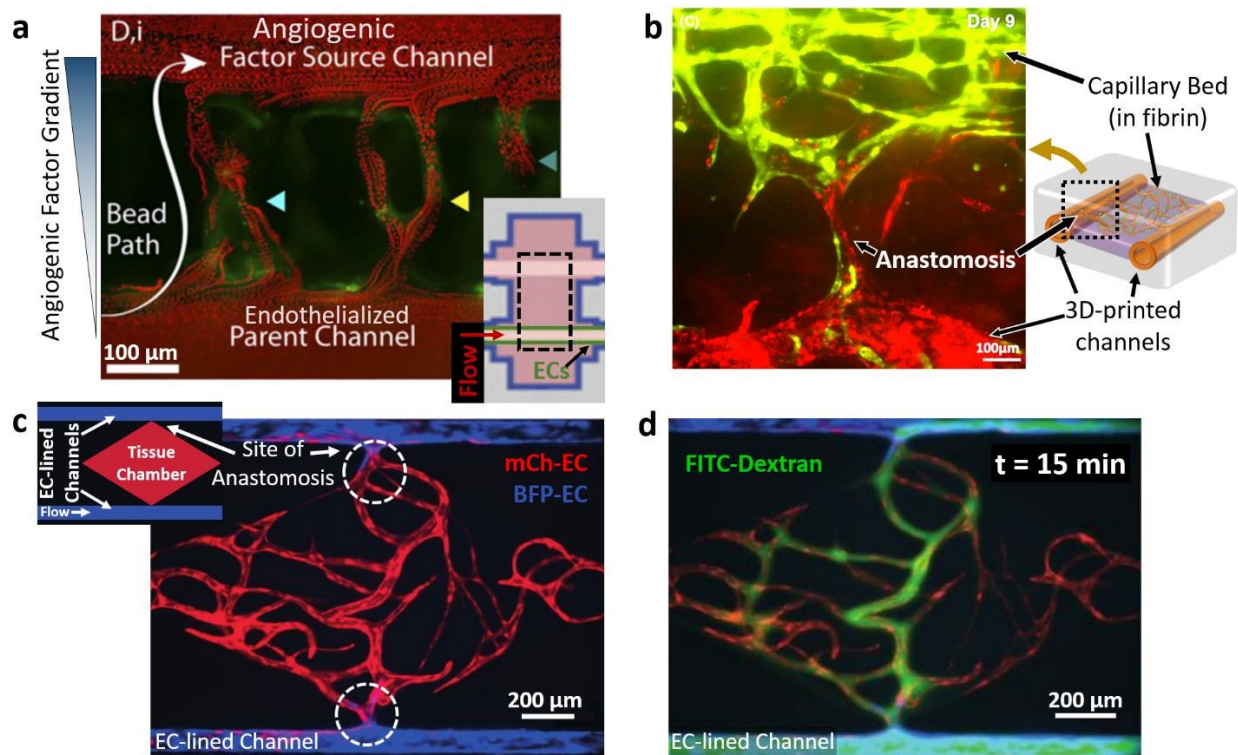


**Fig 6. Establishing multi-scale vasculature in engineered tissue.** a) Sprouting ECs have been observed to create multiscale fluidically connected networks bridging meso-scale networks. Factor source channel refers to the source of angiogenic factors. Here, the red signal is a time-lapse image of fluorescent beads flowing through the connected sprouts. Inset: schematic of microfluidic device indicating the magnified region.<sup>132</sup> b) ECs sprouting off of 3D-printed channels interact with ECs undergoing vasculogenesis in the bulk ECM. The authors subsequently showed fluidic connectivity of these interactions, indicating anastomosis.<sup>134</sup> c) Interaction between angiogenic and vasculogenic ECs (dashed circles) was observed when a capillary bed was allowed to develop adjacent to a meso-scale vessel cultured under flow perfusion. Inset schematic shows the microfluidic device used for the experiment; endothelial cells in the microfluidic channels and tissue chamber were labeled blue and red, respectively. d) Perfusion of the network with fluorescent dextran illustrated fluidic connectivity and therefore anastomosis.<sup>159</sup> Adapted with permission from the National Academy of Science (a), Springer International Publishing Company (b), and the Royal Society of Chemistry (c,d).

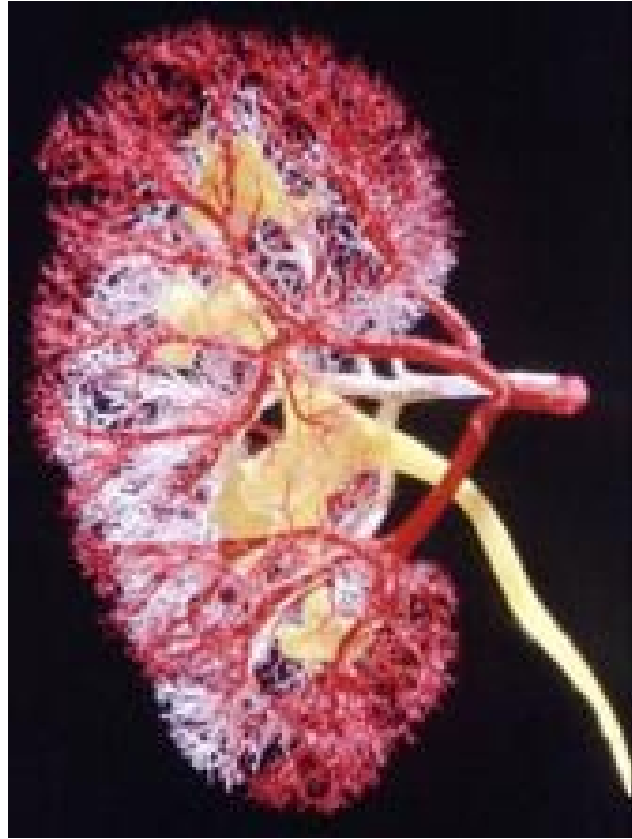


**Fig 7. Interpenetrating networks in human anatomy.** Corrosion cast of the human kidney microvasculature and collecting duct system underscores the highly branched, multiscale, and interpenetrating architecture of native vasculature. Red and white resins were injected into the anterior and posterior branches of the renal artery, respectively, while yellow resin was injected into the ureter. Image courtesy of AO Surgery Reference, [www.aosurgery.org](http://www.aosurgery.org), reprinted with permission; copyright by AO Foundation, Switzerland.



## References

- 1 F. A. Auger, L. Gibot and D. Lacroix, *Annu. Rev. Biomed. Eng.*, 2013, **15**, 177–200.
- 2 T. Kaully, K. Kaufman-Francis, A. Lesman and S. Levenberg, *Tissue Eng. Part B*, 2009.
- 3 E. C. Novosel, C. Kleinhans and P. J. Kluger, *Adv. Drug Deliv. Rev.*, 2011, **63**, 300–311.
- 4 J. S. Miller, *PLoS Biol.*, 2014, **12**, 1–9.
- 5 J. Tien, *Curr. Opin. Chem. Eng.*, 2014, **3**, 36–41.
- 6 Q. Smith and S. Gerecht, *Curr. Opin. Chem. Eng.*, 2014, **3**, 42–50.
- 7 K. H. K. Wong, J. M. Chan, R. D. Kamm and J. Tien, *Annu. Rev. Biomed. Eng.*, 2012, **14**, 205–230.
- 8 S. N. Bhatia and D. E. Ingber, *Nat. Biotechnol.*, 2014, **32**, 760–772.
- 9 N. K. Inamdar and J. T. Borenstein, *Curr. Opin. Biotechnol.*, 2011, **22**, 681–689.
- 10 R. E. Saunders and B. Derby, *Int. Mater. Rev.*, 2014, **59**, 430–448.
- 11 I. T. Ozbolat and M. Hospodiuk, *Biomaterials*, 2016, **76**, 321–343.
- 12 A. Mazzoli, *Med. Biol. Eng. Comput.*, 2013, **51**, 245–256.
- 13 S. F. S. Shirazi, S. Gharekhani, M. Mehrali, H. Yarmand, H. S. C. Metselaar, N. Adib Kadri and N. A. A. Osman, *Sci. Technol. Adv. Mater.*, 2015, **16**, 033502.
- 14 B. Dhariwala, E. Hunt and T. Boland, *Tissue Eng.*, 2004, **10**, 1316–1322.
- 15 L. E. Niklason, J. Gao, W. M. Abbott, K. K. Hirschi, S. Houser, R. Marini and R. Langer, *Science*, 1999, **284**, 489–493.
- 16 E. D. Boland, J. A. Matthews, K. J. Pawlowski, D. G. Simpson, G. E. Wnek and G. L. Bowlin, *Front. Biosci.*, 2004, **9**, 1422–1432.
- 17 S. J. Lee, J. J. Yoo, G. J. Lim, A. Atala and J. Stitzel, *J. Biomed. Mater. Res. Part A*, 2007, **83**, 999–1008.
- 18 N. L'Heureux, N. Dusserre, G. Konig, B. Victor, P. Keire, T. N. Wight, N. A. F. Chronos, A. E. Kyles, C. R. Gregory, G. Hoyt, R. C. Robbins and T. N. McAllister, *Nat. Med.*, 2006, **12**, 361–365.
- 19 J. W. Bjork and R. T. Tranquillo, *Biotechnol. Bioeng.*, 2009, **104**, 1197–206.
- 20 Z. H. Syedain and R. T. Tranquillo, *Biomaterials*, 2009, **30**, 4078–4084.
- 21 C. Norotte, F. S. Marga, L. E. Niklason and G. Forgacs, *Biomaterials*, 2009, **30**, 5910–5917.
- 22 C. Xu, W. Chai, Y. Huang and R. R. Markwald, *Biotechnol. Bioeng.*, 2012, **109**, 3152–3160.

- 23 L. E. Niklason, W. Abbott, J. Gao, B. Klagges, K. K. Hirschi, K. Ulubayram, N. Conroy, R. Jones, A. Vasanawala, S. Sanzgiri and R. Langer, *J. Vasc. Surg.*, 2001, **33**, 628–638.
- 24 N. Koike, D. Fukumura, O. Gralla, P. Au, J. S. Schechner and R. K. Jain, *Nature*, 2004, **428**, 138–139.
- 25 J. J. Moon, J. E. Saik, R. A. Poché, J. E. Leslie-Barbick, S. H. Lee, A. A. Smith, M. E. Dickinson and J. L. West, *Biomaterials*, 2010, **31**, 3840–3847.
- 26 J. S. Jeon, S. Bersini, M. Gilardi, G. Dubini, J. L. Charest, M. Moretti and R. D. Kamm, *Proc. Natl. Acad. Sci. U. S. A.*, 2015, **112**, 214–9.
- 27 D. Therriault, R. F. Shepherd, S. R. White and J. A. Lewis, *Adv. Mater.*, 2005, **17**, 395–399.
- 28 D. Therriault, S. R. White and J. a Lewis, *Nat. Mater.*, 2003, **2**, 265–271.
- 29 W. Wu, C. J. Hansen, A. M. Aragón, P. H. Geubelle, S. R. White and J. A. Lewis, *Soft Matter*, 2010, **6**, 739.
- 30 C. J. Hansen, W. Wu, K. S. Toohey, N. R. Sottos, S. R. White and J. A. Lewis, *Adv. Mater.*, 2009, **21**, 4143–4147.
- 31 C. J. Hansen, S. R. White, N. R. Sottos and J. A. Lewis, *Adv. Funct. Mater.*, 2011, **21**, 4320–4326.
- 32 W. Wu, A. Deconinck and J. A. Lewis, *Adv. Mater.*, 2011, **23**, 1–6.
- 33 G. M. Gratson, M. Xi and J. A. Lewis, *Nature*, 2004, **428**, 386.
- 34 D. Irimia, D. A. Geba and M. Toner, *Anal. Chem.*, 2006, **78**, 3472–3477.
- 35 S. K. W. Dertinger, D. T. Chiu, Noo Li Jeon and G. M. Whitesides, *Anal. Chem.*, 2001, **73**, 1240–1246.
- 36 S. S. Verbridge, A. Chakrabarti, P. Delnero, B. Kwee, J. D. Varner, A. D. Stroock and C. Fischbach, *J. Biomed. Mater. Res. - Part A*, 2013, **101**, 2948–2956.
- 37 N. W. Choi, M. Cabodi, B. Held, J. P. Gleghorn, L. J. Bonassar and A. D. Stroock, *Nat. Mater.*, 2007, **6**, 908–915.
- 38 Y. Xia and G. M. Whitesides, *Annu. Rev. Mater. Sci.*, 1998, **28**, 153–184.
- 39 A. K. Au, N. Bhattacharjee, L. F. Horowitz, T. C. Chang and A. Folch, *Lab Chip*, 2015, **15**, 1934–41.
- 40 P. Tseng, C. Murray, D. Kim and D. Di Carlo, *Lab Chip*, 2014, **14**, 1491–5.
- 41 C. M. B. Ho, S. H. Ng, K. H. H. Li and Y.-J. Yoon, *Lab Chip*, 2015, **15**, 3627–3637.
- 42 A. K. Au, W. Huynh, L. F. Horowitz, A. Folch and A. K. Au, *Angew. Chem. Int. Ed.*, 2016, **55**, 2–22.
- 43 K. S. Toohey, N. R. Sottos, J. A. Lewis, J. S. Moore and S. R. White, *Nat. Mater.*, 2007, **6**, 581–585.

- 44 A. R. Hamilton, N. R. Sottos and S. R. White, *Adv. Mater.*, 2010, **22**, 5159–5163.
- 45 V. L. Tsang, A. A. Chen, L. M. Cho, K. D. Jadin, R. L. Sah, S. DeLong, J. L. West and S. N. Bhatia, *FASEB J.*, 2007, **21**, 790–801.
- 46 J. A. Shepard Neiman, R. Raman, V. Chan, M. G. Rhoads, M. S. B. Raredon, J. J. Velazquez, R. L. Dyer, R. Bashir, P. T. Hammond and L. G. Griffith, *Biotechnol. Bioeng.*, 2014, **112**, 1–33.
- 47 S. J. Hollister, *Nat. Mater.*, 2005, **4**, 518–524.
- 48 S. Wu, X. Liu, K. W. K. Yeung, C. Liu and X. Yang, *Mater. Sci. Eng. R Reports*, 2014, **80**, 1–36.
- 49 S. Bose, M. Roy and A. Bandyopadhyay, *Trends Biotechnol.*, 2012, **30**, 546–554.
- 50 K. M. Chrobak, D. R. Potter and J. Tien, *Microvasc. Res.*, 2006, **71**, 185–196.
- 51 P. A. Galie, D.-H. T. Nguyen, C. K. Choi, D. M. Cohen, P. a Janmey and C. S. Chen, *Proc. Natl. Acad. Sci. U. S. A.*, 2014, **111**, 7968–73.
- 52 K. H. K. Wong, J. G. Truslow and J. Tien, *Biomaterials*, 2010, **31**, 4706–4714.
- 53 J. G. Truslow, G. M. Price and J. Tien, *Biomaterials*, 2009, **30**, 4435–4443.
- 54 M. Cabodi, N. W. Choi, J. P. Gleghorn, C. S. D. Lee, L. J. Bonassar and A. D. Stroock, *J. Am. Chem. Soc.*, 2005, **127**, 13788–13789.
- 55 J. P. Morgan, P. F. Delnero, Y. Zheng, S. S. Verbridge, J. Chen, M. Craven, N. W. Choi, A. Diaz-Santana, P. Kermani, B. Hempstead, J. A. López, T. N. Corso, C. Fischbach and A. D. Stroock, *Nat. Protoc.*, 2013, **8**, 1820–1836.
- 56 S. S. Verbridge, N. W. Choi, Y. Zheng, D. J. Brooks, A. D. Stroock and C. Fischbach, *Tissue Eng. Part A*, 2010, **16**, 2133–41.
- 57 Y. Zheng, J. Chen, M. Craven, N. W. Choi, S. Totorica, A. Diaz-Santana, P. Kermani, B. Hempstead, C. Fischbach-Teschl, J. A. Lopez and a. D. Stroock, *Proc. Natl. Acad. Sci.*, 2012, **109**, 9342–9347.
- 58 K. R. King, C. C. J. Wang, M. R. Kaazempur-Mofrad, J. P. Vacanti and J. T. Borenstein, *Adv. Mater.*, 2004, **16**, 2007–2012.
- 59 A. P. Golden and J. Tien, *Lab Chip*, 2007, **7**, 720.
- 60 Y. Zheng, J. Chen and J. A. López, *Thromb. Res.*, 2014, **133**, 525–531.
- 61 J. V Green, T. Kniazeva, M. Abedi, D. S. Sokhey, M. E. Taslim and S. K. Murthy, *Lab Chip*, 2009, **9**, 677–685.
- 62 L. K. Fiddes, N. Raz, S. Srigunapalan, E. Tumarkan, C. A. Simmons, A. R. Wheeler and E. Kumacheva, *Biomaterials*, 2010, **31**, 3459–3464.
- 63 T. J. Hinton, Q. Jallerat, R. N. Palchesko, J. H. Park, M. S. Grodzicki, H. Shue, M. H. Ramadan, A. R. Hudson and A. W. Feinberg, *Sci. Adv.*, 2015.

- 64 J. S. Miller, K. R. Stevens, M. T. Yang, B. M. Baker, D.-H. T. Nguyen, D. M. Cohen, E. Toro, A. A. Chen, P. A. Galie, X. Yu, R. Chaturvedi, S. N. Bhatia and C. S. Chen, *Nat. Mater.*, 2012, **11**, 768–774.
- 65 H. Lin, D. Zhang, P. G. Alexander, G. Yang, J. Tan, A. W. M. Cheng and R. S. Tuan, *Biomaterials*, 2013, **34**, 331–339.
- 66 L. Zhao, V. K. Lee, S. S. Yoo, G. Dai and X. Intes, *Biomaterials*, 2012, **33**, 5325–5332.
- 67 V. K. Lee, D. Y. Kim, H. Ngo, Y. Lee, L. Seo, S. S. Yoo, P. A. Vincent and G. Dai, *Biomaterials*, 2014, **35**, 8092–8102.
- 68 S. Wüst, R. Müller and S. Hofmann, *J. Biomed. Mater. ...*, 2014, 1–13.
- 69 K. Arcaute, B. K. Mann and R. B. Wicker, *Ann. Biomed. Eng.*, 2006, **34**, 1429–1441.
- 70 K. Arcaute, B. K. Mann and R. B. Wicker, *Acta Biomater.*, 2010, **6**, 1047–1054.
- 71 S. Suri, L.-H. Han, W. Zhang, A. Singh, S. Chen and C. E. Schmidt, *Biomed. Microdevices*, 2011, **13**, 983–993.
- 72 R. Raman, B. Bhaduri, M. Mir, A. Shkumatov, M. K. Lee, G. Popescu, H. Kong and R. Bashir, *Adv. Healthc. Mater.*, 2015, n/a–n/a.
- 73 J. R. Tumbleston, D. Shirvanyants, N. Ermoshkin, A. R. Johnson, D. Kelly, K. Chen, R. Pinschmidt, J. P. Rolland, A. Ermoshkin, E. T. Samulski and M. Joseph, *Science (80-. )*, 2015, 1–7.
- 74 K. C. Hribar, D. Finlay, X. Ma, X. Qu, M. G. Ondeck, P. H. Chung, F. Zanella, A. J. Engler, F. Sheikh, K. Vuori and S. C. Chen, *Lab Chip*, 2015, **15**, 2412–2418.
- 75 Y. Zhang, Y. Yu and I. T. Ozbolat, *J. Nanotechnol. Eng. Med.*, 2013, **4**, 020902.
- 76 Y. Zhang, Y. Yu, H. Chen and I. T. Ozbolat, *Biofabrication*, 2013, **5**, 025004.
- 77 Y. Zhang, Y. Yu, A. Akkouch, A. Dababneh, F. Dolati and I. T. Ozbolat, *Biomater. Sci.*, 2015, **3**, 134–143.
- 78 Q. Gao, Y. He, J. Fu, A. Liu and L. Ma, *Biomaterials*, 2015, **61**, 203–215.
- 79 Y. Luo, A. Lode and M. Gelinsky, *Adv. Healthc. Mater.*, 2013, **2**, 777–83.
- 80 C. Colosi, S. R. Shin, V. Manoharan, S. Massa, M. Costantini, A. Barbetta, M. R. Dokmeci, M. Dentini and A. Khademhosseini, *Adv. Mater.*, 2015, n/a–n/a.
- 81 C. D. Murray, *J. Gen. Physiol.*, 1926, **9**, 835–841.
- 82 T. F. Sherman, *J. Gen. Physiol.*, 1981, **78**, 431–453.
- 83 K. Christensen, C. Xu, W. Chai, Z. Zhang, J. Fu and Y. Huang, *Biotechnol. Bioeng.*, 2015, **112**, 1047–55.
- 84 W. Meyer, S. Engelhardt, E. Novosel, B. Elling, M. Wegener and H. Krüger, *J. Funct. Biomater.*, 2012, **3**, 257–68.

- 85 T. Bhattacharjee, S. M. Zehnder, K. G. Rowe, S. Jain, R. M. Nixon, W. G. Sawyer and T. E. Angelini, *Sci. Adv.*, 2015, 1–7.
- 86 A. J. Liu and S. R. Nagel, *Annu. Rev. Condens. Matter Phys.*, 2010, **1**, 347–369.
- 87 L. E. Bertassoni, M. Cecconi, V. Manoharan, M. Nikkhah, J. Hjortnaes, A. L. Cristino, G. Barabaschi, D. Demarchi, M. R. Dokmeci, Y. Yang and A. Khademhosseini, *Lab Chip*, 2014, **14**, 2202–11.
- 88 D. B. Kolesky, R. L. Truby, a. S. Gladman, T. A. Busbee, K. A. Homan and J. A. Lewis, *Adv. Mater.*, 2014, **26**, 3124–3130.
- 89 D. B. Kolesky, K. A. Homan, M. A. Skylar-Scott and J. A. Lewis, *Proc. Natl. Acad. Sci.*, 2016, 201521342.
- 90 H.-W. Kang, S. J. Lee, I. K. Ko, C. Kengla, J. J. Yoo and A. Atala, *Nat. Biotechnol.*, 2016, 3–7.
- 91 P. A. Galie, A. van Oosten, C. S. Chen and P. A. Janmey, *Lab Chip*, 2015, **15**, 1205–1212.
- 92 A. Qutub, F. Gabhann, E. Karagiannis, P. Vempati and A. Popel, *IEEE Eng. Med. Biol. Mag.*, 2009, **28**, 14–31.
- 93 R. Rekhi and A. A. Qutub, *Front. Physiol.*, 2013, **4**, 285.
- 94 A. D. Leung, K. H. K. Wong and J. Tien, *J. Biomed. Mater. Res. - Part A*, 2012, **100 A**, 1815–1822.
- 95 G. M. Price, K. M. Chrobak and J. Tien, *Microvasc. Res.*, 2008, **76**, 46–51.
- 96 R. H. Adamson, B. Liu, G. N. Fry, L. L. Rubin and F. E. Curry, *Am. J. Physiol.*, 1998, **274**, H1885–94.
- 97 A. P. McGuigan and M. V. Sefton, *Biomaterials*, 2007, **28**, 2547–2571.
- 98 A. P. McGuigan and M. V. Sefton, *Biomaterials*, 2008, **29**, 2453–63.
- 99 Z. M. Ruggeri, *Microcirculation*, 2009, **16**, 58–83.
- 100 M. H. Kroll, J. D. Hellums, L. V. McIntire, A. I. Schafer and J. L. Moake, *Blood*, 1991, **78**, 1–19.
- 101 R. Sooppan, S. J. Paulsen, J. Han, A. H. Ta, P. Dinh, A. C. Gaffey, C. Venkataraman, A. Trubelja, G. Hung, J. S. Miller and P. Atluri, *Tissue Eng. Part C Methods*, 2015, **22**, ten.tec.2015.0239.
- 102 D. a Boas and A. K. Dunn, *J. Biomed. Opt.*, 2014, **15**, 011109.
- 103 G. Cheng, S. Liao, H. K. Wong, D. a. Lacorre, E. Di Tomaso, P. Au, D. Fukumura, R. K. Jain and L. L. Munn, *Blood*, 2011, **118**, 4740–4749.
- 104 S. Levenberg, J. Rouwkema, M. Macdonald, E. S. Garfein, D. S. Kohane, D. C. Darland, R. Marini, C. A. van Blitterswijk, R. C. Mulligan, P. A. D’Amore and R. Langer, *Nat. Biotechnol.*, 2005, **23**, 879–884.

- 105 A. Diaz-Santana, M. Shan and A. D. Stroock, *Integr. Biol.*, 2015, **7**, 454–466.
- 106 K. Gaengel, G. Genove, A. Armulik and C. Betsholtz, *Arterioscler. Thromb. Vasc. Biol.*, 2009, **29**, 630–638.
- 107 A. N. Stratman and G. E. Davis, *Microsc. Microanal.*, 2013, **18**, 1199–1216.
- 108 G. Bergers, *Neuro. Oncol.*, 2005, **7**, 452–464.
- 109 N. P. J. Brindle, *Circ. Res.*, 2006, **98**, 1014–1023.
- 110 S. K. Ramasamy, A. P. Kusumbe and R. H. Adams, *Trends Cell Biol.*, 2015, **25**, 148–157.
- 111 S. Rafii, J. M. Butler and B.-S. Ding, *Nature*, 2016, **529**, 316–325.
- 112 E. Lammert, O. Cleaver and D. Melton, *Science (80-. )*, 2001, **294**, 564–567.
- 113 J. LeCouter, D. R. Moritz, B. Li, G. L. Phillips, X. H. Liang, H.-P. Gerber, K. J. Hillan and N. Ferrara, *Science (80-. )*, 2003, **299**, 890–893.
- 114 M. A. Swartz and M. E. Fleury, *Annu. Rev. Biomed. Eng.*, 2007, **9**, 229–256.
- 115 J. M. Rutkowski and M. a. Swartz, *Trends Cell Biol.*, 2007, **17**, 44–50.
- 116 C. P. Ng and M. A. Swartz, *Am. J. Physiol. Heart Circ. Physiol.*, 2003, **284**, H1771–7.
- 117 C. P. Ng, B. Hinz and M. A. Swartz, *J. Cell Sci.*, 2005, **118**, 4731–4739.
- 118 C. P. Ng, C. L. E. Helm and M. A. Swartz, *Microvasc. Res.*, 2004, **68**, 258–264.
- 119 K. H. Benam, S. Dauth, B. Hassell, A. Herland, A. Jain, K.-J. Jang, K. Karalis, H. J. Kim, L. MacQueen, R. Mahmoodian, S. Musah, Y.-S. Torisawa, A. D. van der Meer, R. Villenave, M. Yadid, K. K. Parker and D. E. Ingber, *Annu. Rev. Pathol.*, 2015, **10**, 195–262.
- 120 C. M. Ghajar and M. J. Bissell, *Tissue Eng. Part A*, 2010, **16**, 2153–2156.
- 121 J. S. Jeon, I. K. Zervantonakis, S. Chung, R. D. Kamm and J. L. Charest, *PLoS One*, 2013, **8**, e56910.
- 122 I. K. Zervantonakis, S. K. Hughes-Alford, J. L. Charest, J. S. Condeelis, F. B. Gertler and R. D. Kamm, *Proc. Natl. Acad. Sci.*, 2012, **109**, 13515–13520.
- 123 M. B. Chen, J. a Whisler, J. S. Jeon and R. D. Kamm, *Integr. Biol. (Camb.)*, 2013, **5**, 1262–71.
- 124 R. Hernández Vera, E. Genové, L. Alvarez, S. Borrós, R. Kamm, D. Lauffenburger and C. E. Semino, *Tissue Eng. Part A*, 2009, **15**, 175–85.
- 125 J. L. Albritton, J. D. Roybal, S. J. Paulsen, N. Calafat, J. A. Flores-Zaher, M. C. Farach-Carson, D. L. Gibbons and J. S. Miller, *RSC Adv.*, 2016, **6**, 8980–8991.
- 126 P. Koumoutsakos, I. Pivkin and F. Milde, *Annu. Rev. Fluid Mech.*, 2013, **45**, 325–355.
- 127 D. W. Siemann, *Cancer Treat. Rev.*, 2011, **37**, 63–74.

- 128 T. Stylianopoulos and R. K. Jain, *Proc. Natl. Acad. Sci. U. S. A.*, 2013, **110**, 18632–7.
- 129 L. Y. Di Marco, A. Venneri, E. Farkas, P. C. Evans, A. Marzo and A. F. Frangi, *Neurobiol. Dis.*, 2015, **82**, 593–606.
- 130 H. P. Hammes, J. Lin, P. Wagner, Y. Feng, F. Vom Hagen, T. Krzizok, O. Renner, G. Breier, M. Brownlee and U. Deutsch, *Diabetes*, 2004, **53**, 1104–1110.
- 131 A. Atala, F. K. Kasper and A. G. Mikos, *Sci. Transl. Med.*, 2012, **4**, 160rv12–160rv12.
- 132 D.-H. T. Nguyen, S. C. Stapleton, M. T. Yang, S. S. Cha, C. K. Choi, P. A. Galie and C. S. Chen, *Proc. Natl. Acad. Sci.*, 2013, **110**, 6712–6717.
- 133 J. A. Whisler, M. B. Chen and R. D. Kamm, *Tissue Eng. Part C. Methods*, 2014, **20**, 543–52.
- 134 V. K. Lee, A. M. Lanzi, H. Ngo, S. S. Yoo, P. a. Vincent and G. Dai, *Cell. Mol. Bioeng.*, 2014, **7**, 460–472.
- 135 X. Wang, D. T. T. Phan, S. C. George, C. C. W. Hughes and A. P. Lee, *Lab Chip*, 2015.
- 136 M. L. Moya, Y.-H. Hsu, A. P. Lee, C. C. W. Hughes and S. C. George, *Tissue Eng. Part C Methods*, 2013, **19**, 730–737.
- 137 Y.-H. Hsu, M. L. Moya, C. C. W. Hughes, S. C. George and A. P. Lee, *Lab Chip*, 2013, **13**, 2990.
- 138 R. S. Udan, T. J. Vadakkan and M. E. Dickinson, *Development*, 2013, **140**, 4041–50.
- 139 M. A. Swartz, A. Kaipainen, P. A. Netti, C. Brekken, Y. Boucher, A. J. Grodzinsky and R. K. Jain, *J. Biomech.*, 1999, **32**, 1297–1307.
- 140 K. H. K. Wong, J. G. Truslow, A. H. Khankhel, K. L. S. Chan and J. Tien, *J. Biomed. Mater. Res. - Part A*, 2013, **101 A**, 2181–2190.
- 141 I. S. Kinstlinger, A. Bastian, S. J. Paulsen, D. H. Hwang, A. H. Ta, D. R. Yalacki, T. Schmidt and J. S. Miller, *PLoS One*, 2016, **11**, e0147399.
- 142 A. A. Linninger, I. G. Gould, T. Marinnan, C. Y. Hsu, M. Chojecki and A. Alaraj, *Ann. Biomed. Eng.*, 2013, **41**, 2264–2284.
- 143 S. J. Paulsen and J. S. Miller, *Dev. Dyn.*, 2015, n/a–n/a.
- 144 D. J. Beebe, G. A. Mensing and G. M. Walker, *Annu. Rev. Biomed. Eng.*, 2002, **4**, 261–286.
- 145 K. A. McCulloh, J. S. Sperry and F. R. Adler, *Nature*, 2003, **421**, 939–942.
- 146 Y. Zhou, G. S. Kassab and S. Molloi, *Phys. Med. Biol.*, 1999, **2929**, 2929–2945.
- 147 Y. Nakamura and S. Awa, *Physiol. Rep.*, 2014, **2**, e00236.
- 148 G. S. Kassab, *Am. J. Physiol. Heart Circ. Physiol.*, 2006, **290**, H894–H903.
- 149 N. Chapman, G. Dell’omo, M. S. Sartini, N. Witt, a Hughes, S. Thom and R. Pedrinelli,

- Clin. Sci. (Lond).*, 2002, **103**, 111–6.
- 150 N. Witt, T. Y. Wong, A. D. Hughes, N. Chaturvedi, B. E. Klein, R. Evans, M. McNamara, S. A. McG Thom and R. Klein, *Hypertension*, 2006, **47**, 975–981.
- 151 K. T. Nguyen, C. D. Clark, T. J. Chancellor and D. V. Papavassiliou, *J. Biomech.*, 2008, **41**, 11–19.
- 152 E. Cecchi, C. Giglioli, S. Valente, C. Lazzeri, G. F. Gensini, R. Abbate and L. Mannini, *Atherosclerosis*, 2011, **214**, 249–256.
- 153 C. K. Zarins, D. P. Giddens, B. K. Bharadvaj, V. S. Sottiurai, R. F. Mabon, S. Gladov and S. Glagov, *Circ. Res.*, 1983, **53**, 502–514.
- 154 P. A. Galie, D.-H. T. Nguyen, C. K. Choi, D. M. Cohen, P. a Janmey and C. S. Chen, *Proc. Natl. Acad. Sci. U. S. A.*, 2014, **111**, 7968–73.
- 155 D. Goldman and A. S. Popel, *J. Theor. Biol.*, 2000, **206**, 181–194.
- 156 E. Bullitt, K. E. Muller, I. Jung, W. Lin and S. Aylward, *Med. Image Anal.*, 2005, **9**, 39–49.
- 157 S. L. Faley, B. B. Baer, T. S. H. Larsen and L. M. Bellan, *Biomicrofluidics*, 2015, **9**, 036501.
- 158 S. Lee, C. Vinegoni, P. F. Feruglio, L. Fexon, R. Gorbato, M. Pivoravov, A. Sbarbati, M. Nahrendorf and R. Weissleder, *Nat. Commun.*, 2012, **3**, 1054.
- 159 X. Wang, D. T. T. Phan, S. C. George, C. C. W. Hughes and A. P. Lee, *Lab Chip*, 2015.